Accepted Manuscript

Second generation of diazachrysenes: Protection of Ebola virus infected mice and mechanism of action

Života Selaković, Julie P. Tran, Krishna P. Kota, Marija Lazić, Cary Retterer, Robert Besh, Rekha G. Panchal, Veronica Soloveva, Vantongreen A. Sean, Wells B. Jay, Aleksandar Pavić, Tatjana Verbić, Branka Vasiljević, Kathleen Kuehl, Allen J. Duplantier, Sina Bavari, Rajini Mudhasani, Bogdan A. Šolaja

PII: S0223-5234(18)30938-3

DOI: https://doi.org/10.1016/j.ejmech.2018.10.061

Reference: EJMECH 10847

To appear in: *European Journal of Medicinal Chemistry*

Received Date: 6 September 2018

Revised Date: 17 October 2018

Accepted Date: 27 October 2018

Please cite this article as: Ž. Selaković, J.P. Tran, K.P. Kota, M. Lazić, C. Retterer, R. Besh, R.G. Panchal, V. Soloveva, V.A. Sean, W.B. Jay, A. Pavić, T. Verbić, B. Vasiljević, K. Kuehl, A.J. Duplantier, S. Bavari, R. Mudhasani, B.A. Šolaja, Second generation of diazachrysenes: Protection of Ebola virus infected mice and mechanism of action, *European Journal of Medicinal Chemistry* (2018), doi: https://doi.org/10.1016/j.ejmech.2018.10.061.

This is a PDF file of an unedited manuscript that has been accepted for publication. As a service to our customers we are providing this early version of the manuscript. The manuscript will undergo copyediting, typesetting, and review of the resulting proof before it is published in its final form. Please note that during the production process errors may be discovered which could affect the content, and all legal disclaimers that apply to the journal pertain.

View metadata, citation and similar papers at core.ac.uk

brought to you by CORE

provided by Faculty of Chemistry Repository - Chemy

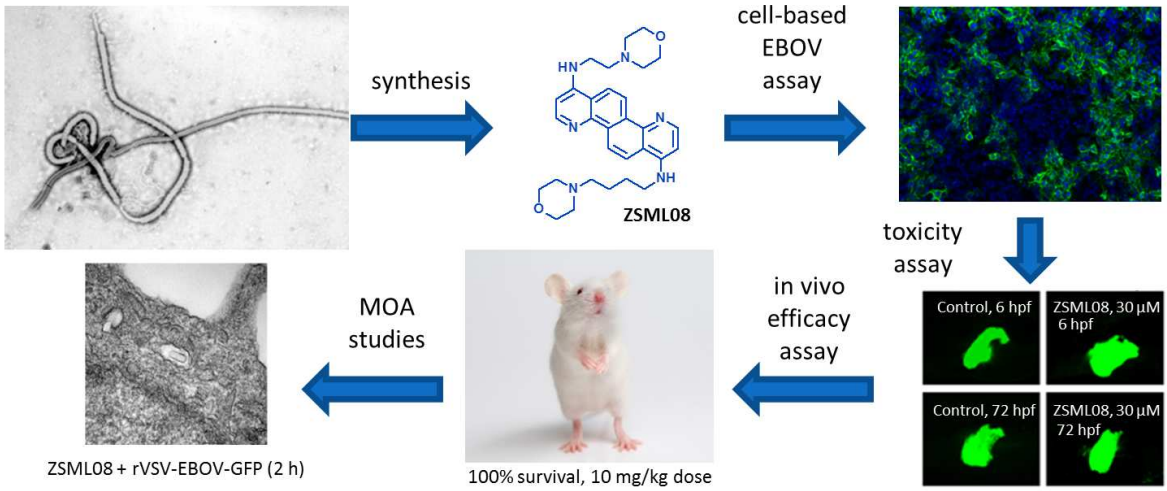

ACCEPTED MANUSCRIPT

ACCEPTED MANUSCRIPT

Second generation of diazachrysenes: protection of Ebola virus infected mice and mechanism of action

Života Selaković,[#] Julie P. Tran,[‡] Krishna P. Kota,[‡] Marija Lazić,[#] Cary Retterer,[‡] Robert Besh,[‡] Rekha G. Panchal,[‡] Veronica Soloveva,[‡] Vantongreen A. Sean,[‡] Wells B. Jay,[‡] Aleksandar Pavić,[¶] Tatjana Verbić,[#] Branka Vasiljević,[¶] Kathleen Kuehl,[‡] Allen J. Duplantier,[‡] Sina Bavari,[‡] Rajini Mudhasani,[‡,∇,] Bogdan A. Šolaja[#,§,*]*

[#] University of Belgrade, Faculty of Chemistry, Studentski trg 12-16, P.O. Box 51, 11158, Belgrade, Serbia

[‡] Molecular and Translational Sciences Division, United States Army Medical Research Institute of Infectious Diseases, 1425 Porter Street, Frederick, Maryland 21702, United States

[¶] Institute of Molecular Genetics and Genetic Engineering, University of Belgrade, Belgrade, Serbia

[∇] Department of Pathology and Microbiology, University of Nebraska Medical Center, 985900 Nebraska Medical Center, Omaha, NE 68198-5900, United States

[§] Serbian Academy of Sciences and Arts, Knez Mihailova 35, 11158 Belgrade, Serbia

*Corresponding authors

Keywords: diazachrysene filovirus inhibitors, naphthyridines, Ebola virus entry inhibitors, late endosomes, lysosomotroph

ABSTRACT

Ebola virus (EBOV) causes a deadly hemorrhagic fever in humans and non-human primates. There is currently no FDA-approved vaccine or medication to counter this disease. Here, we report on the design, synthesis and anti-viral activities of two classes of compounds which show high potency against EBOV in both in vitro cell culture assays and in vivo mouse models Ebola viral disease. These compounds incorporate the structural features of cationic amphiphilic drugs (CAD), i.e they possess both a hydrophobic domain and a hydrophilic domain consisting of an ionizable amine functional group. These structural features enable easily diffusion into cells but once inside an acidic compartment their amine groups became protonated, ionized and remain trapped inside the acidic compartments such as late endosomes and lysosomes. These compounds, by virtue of their lysomotrophic functions, blocked EBOV entry. However, unlike other drugs containing a CAD moiety including chloroquine and amodiaquine, compounds reported in this study display faster kinetics of accumulation in the lysosomes, robust expansion of late endosome/lysosomes, relatively more potent suppression of lysosome fusion with other vesicular compartments and inhibition of cathepsins activities, all of which play a vital role in anti-EBOV activity. Furthermore, the diazachrysene **2** (**ZSML08**) that showed most potent activity against EBOV in in vitro cell culture assays also showed significant survival benefit with 100 percent protection in mouse models of Ebola virus disease, at a low dose of 10 mg/kg/day. Lastly, toxicity studies in vivo using zebrafish models suggest no developmental defects or toxicity associated with these compounds. Overall, these studies describe two new pharmacophores that by virtue of being potent lysosomotrophs, display potent anti-EBOV activities both in vitro and in vivo animal models of EBOV disease.

INTRODUCTION

The latest Ebola virus disease (EVD) epidemic hit West Africa from late 2013 to mid-2016, resulting in more than 11,000 deaths.[1] The average fatality rate (about 40%) was lower than in many of the previous outbreaks (up to 90%). However, the number of cases exceeded all previous outbreaks combined by more than tenfold and the number of deaths by more than sevenfold.[2] A more recent outbreak has been reported in West Africa with a total of 78 cases of hemorrhagic fever, including 44 deaths so far.[3]

EBOV is a single-stranded, negative sense RNA virus and is a member of the genus *Ebolavirus* in the family *Filoviridae*. It is closely related to Marburg virus, which, like Ebola Virus (EBOV), causes a hemorrhagic fever in humans and non-human primates.[4] The natural reservoir of filoviruses are possibly bats, albeit transmission to humans can also occur via non-human primates and possibly other animals as well.[5]

Currently there is no FDA licensed drug, vaccine or any other therapeutic to treat EVD.[6] At least three vaccine candidates have shown promising results and have entered clinical trials to various degrees.[7-10][7,8,9,10] The unpredictable nature of occurrence of new outbreaks, followed by a prolonged period usually taken to attribute the patients' symptoms to EVD, often results in rapid spread of the contagion. This underlines the need for a readily available therapeutic, with a long shelf life and one that could be easily stored. Research conducted by different teams,[11-14][11,12,13,14] as well as our own,[15-17][15,16,17] has provided a number of active small molecule EBOV inhibitors, that could meet the aforementioned criteria (Figure 1). Favipiravir, BCX4430 and GS-5734, act as prodrugs that are metabolized into selective EBOV RNA-polymerase inhibitors.[11,12,15,16]

More recently, repurposing drug screens identified small molecules belonging to cationic amphiphilic drugs (CADs) family, as potent inhibitors of EBOV entry.[18-20][18,19,20] CADs are a wide group of chemicals that typically have both a hydrophobic domain containing an aromatic ring system and a hydrophilic domain containing an ionizable amine functional group.[21] These structural features, enables easily diffusion into cells but once inside an acidic compartment their amine groups become protonated, ionized and remain trapped. As a result, CADs are lysosomotropic, i.e., accumulate to high concentrations in the acidic compartments such as Late Endosomes and Lysosomes (LE/Ly) thereby altering their morphology and functions. Regardless of their intended target, many FDA approved drugs with a CAD moiety in their backbone, blocked EBOV entry in *in vitro* assays by altering LE/Ly functions.[13,20]

EBOV entry is exclusively dependent on EBOV Glycoprotein (GP) trimers that project as long spikes on the lipid bilayer envelope. The viral entry begins with the viral attachment to the host cell surface followed by virus internalization through macropinocytosis. The virus is then trafficked sequentially from the early endosomes to the LE and Ly. In the LE/Ly, the cysteine proteases; Cathepsin B and/or Cathepsin L under acidic pH and reducing conditions, cleave GP to generate a 17-19 kDa fusogenic version of GP.[22-24][22,23,24] The cleaved GP also unmasks its binding site to the LE/Ly resident receptor, the Niemann-Pick C1 (NPC1). GP-NPC1 interaction promotes the filovirus/cell membrane fusion, that eventually leads to the release of viral lipid membrane enclosed ribonucleoprotein complex (RNP) into the cytoplasm for transcription.[25,26] For successful entry, trafficking of EBOV virions to specific NPC1 expressing LE/Ly compartments is crucial to promote EBOV fusion with the limiting membrane to release the enclosed nucleocapsid into cytoplasm. CADs appear to block these interactions by modulating the LE/Ly, however the exact mechanism is not known.

In spite of many CADs being effective in vitro in cell culture assays, only few of them were effective in vivo in mouse models of Ebola virus disease. Among the successful ones, chloroquine (**CQ**) and amiodarone at 90 mg/kg, protected mice in one study but failed in another.[18,27-29][18,27,28,29] Amodiaquine (**AQ**) did not protect mice,[29] but its usage in humans during 2014 EBOV outbreak, in place of an antimalarial containing lumefantrine at Médecins Sans Frontières-led treatment units, was associated with an observed decrease in human fatality rates.[30] Toremifene (Figure 1) at 60 mg/kg protected mice but the doses used were higher than what was normally tested for clinical usage and hence is potentially associated with serious side effects.[13] Sertraline offered 70% and Bepridil offered 100% protection of mice at a lower dosage of 20 mg/kg/day and 24 mg/kg/day, respectively.[20] Potency differences may correlate with interactions with lipid and protein moieties within the LE/Ly compartments that ultimately impact EBOV entry. However, the primary intended target of the approved drugs was not to function as CADs and their anti-EBOV activity required several 10-100 higher fold usage of the drug in in vitro studies when compared to their activity against their original intended target. Their application in animal models would require re-testing tolerability at higher doses and are compounded by the complications of their effects on their primary intended targets. Therefore, a more efficient CAD that disrupts EBOV entry without causing any serious side effects would be highly desirable.

ACCEPTED MANUSCRIPT

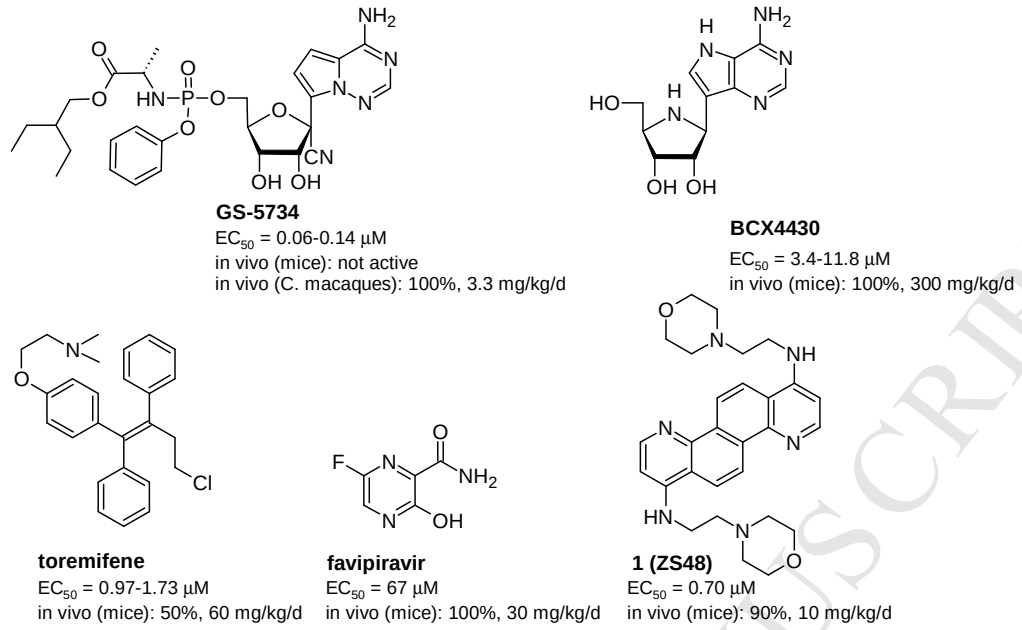

Figure 1. Selected examples of small molecule EBOV inhibitors.

Here, we report on the development of a novel anti-EBOV pharmacophore with a 1,4-naphthyridine core (Chart 1). Furthermore, for the first time the synthesis of diazachrysene derivatives substituted by two different aminoalkyl side chains has been achieved, diverging from **1 (ZS48)** and alike.[17,31] The synthesis, pharmacokinetic analysis, in vitro and in vivo antiviral screening efforts, and detailed mechanism of action (MOA) studies suggest that the studied compounds are CADs with unique features and represent the most potent inhibitors of EBOV within the CAD structural class.

ACCEPTED MANUSCRIPT

Chart 1. General structures of investigated derivatives

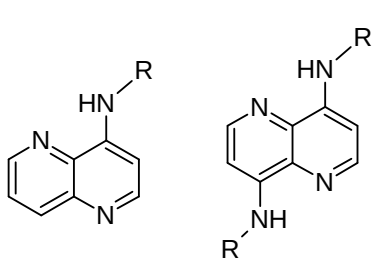

aminoalkyl derivatives of 1,4-naphthyridine

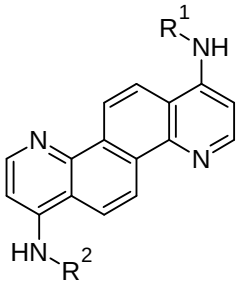

aminoalkyl derivatives of 4,10-diazachrysene with two different substituents

RESULTS AND DISCUSSION

Synthesis

Being aware that increased number of aromatic rings may disfavor our drug development efforts based on 4,10-diazachrysene core,[32] beside extensive toxicity evaluation thereof, we entered the core ring re-grouping to two central aromatic rings aiming at naphthyridine core instead (Figure 2). Furthermore, the envisioned naphthyridine derivatives have a structural similarity to the FDA approved antimalarial drug **CQ**, which was found to have moderate anti-EBOV activity.[18,27] The planned naphthyridine compounds would preserve the 4-alkylaminopyridine constitutional motif, akin to alkylamino substituted 4,10-diazachrysenes, which appears to decrease the susceptibility to metabolic activation and the toxicity proceeding thereof.[31,33]

ACCEPTED MANUSCRIPT

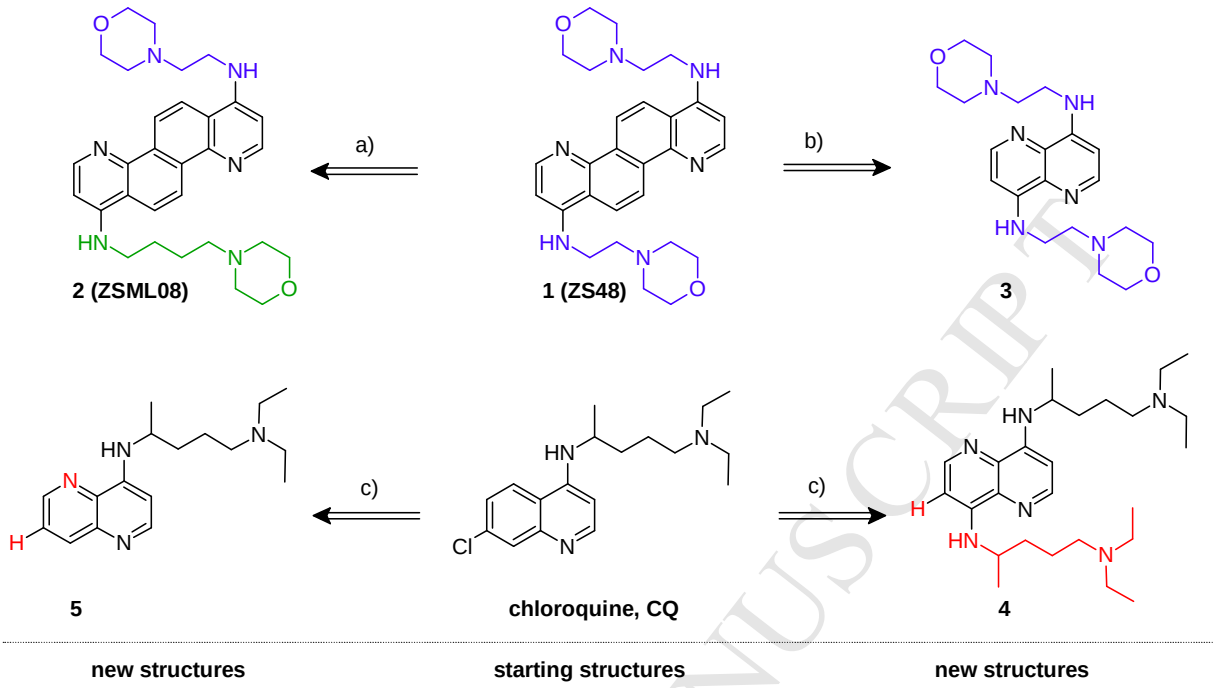

Figure 2. Planned transformations: a) Desymmetrization **1**→**2**; b) Core reduction **1**→**3**; c) **CQ** surrogates.

Firstly, two naphthyridine core compounds, **6**[34,35] and **7**[36-38][36,37,38] were synthesized using slightly modified approaches than those already known (see Supporting Information 1). These two compounds were then subjected to microwave-assisted nucleophilic substitution reactions with appropriate amines. This gave rise to 12 alkylamino substituted compounds (**3-5** and **8-16**, as shown in Scheme 1, thus affording for the first time the 4,8-alkylamino substituted 1,5-naphthyridines.

ACCEPTED MANUSCRIPT

Scheme 1. The synthesis of alkylamino substituted naphthyridines.

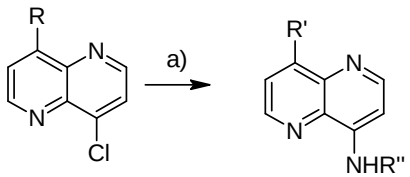

6: R = H
7: R = Cl

a) RNH_2, MW, NMR, 180 ^oC, 2h;

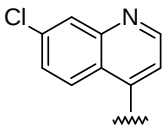

R'''

R' = H

5: R'' = $-CH(CH_3)(CH_2)_3N(CH_2CH_3)_2$, 78%
8: R'' = $-(CH_2)_3N(CH_2CH_2)O$, 91%
9: R'' = $-(CH_2)_3N(CH_2CH_3)_2$, 59%
10: R'' = $-CH_2CH(OH)CH_2N(CH_2CH_3)_2$, 54%
11: R'' = $-(CH_2)_4NHR'''$, 38%

R' = -NHR''

3: R'' = $-(CH_2)_2N(CH_2CH_2)_2O$, 71%
4: R'' = $-CH(CH_3)(CH_2)_3N(CH_2CH_3)_2$, 51%
12: R'' = $-(CH_2)_3N(CH_2CH_2)_2O$, 33%
13: R'' = $-(CH_2)_3N(CH_2CH_3)_2$, 41%
14: R'' = $-CH_2CH(OH)CH_2N(CH_2CH_3)_2$, 67%
15: R'' = $-(CH_2)_2N(CH_2CH_3)_2$, 46%
16: R'' = $-(CH_2)_4N(CH_2CH_2)_2O$, 46%

Our initial diazachrysene structures were substituted with two identical aminoalkyl sidechains.[17] Therefore, for the synthesis of unsymmetrically substituted diazachrysenes, the experience in tuning up the conditions for microwave-assisted nucleophilic aromatic substitution on the diazachrysene core[31] helped us optimize the procedure that resulted in monosubstitution reaction keeping one chloro substituent intact (Scheme 2). The remaining chlorine in **18** was then substituted with different aminoalkyl side-chains. In addition, we synthesized three uniformly substituted derivatives, **21**, **22** and **23**.

ACCEPTED MANUSCRIPT

Scheme 2. The synthesis of alkylamino-substituted diazachrysenes.

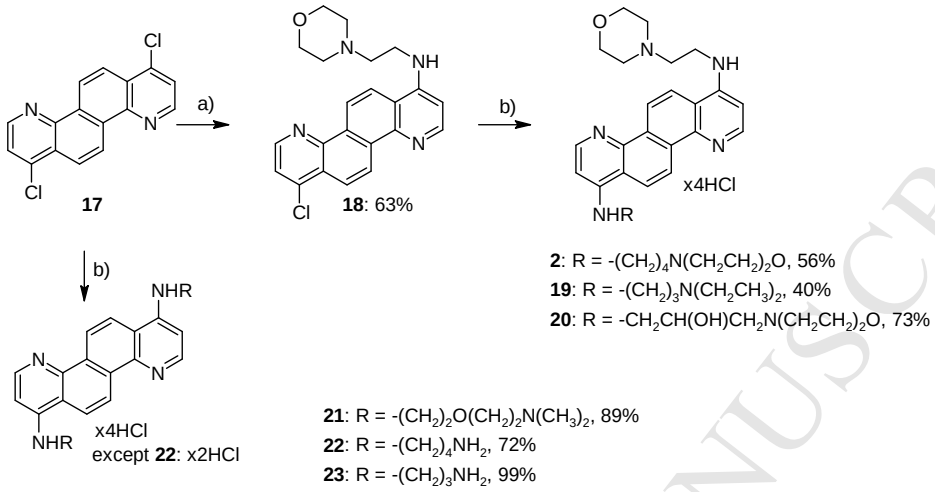

Inhibitory Activity Against EBOV

The compounds were screened for their antiviral activity in cell based High throughput, high Content Imaging (HCI) assay, and their EC_{50} and/or EC_{90} and CC_{50} were assessed by running a dose response curve analysis (Table 1).[39,40] Briefly, HeLa or human foreskin fibroblast (HFF) cells were pretreated with different doses of the compounds for 2 h prior to incubating with EBOV. Forty-eight hours post infection (following multiple cycles of viral infections), cells were subjected to immunofluorescence analysis (IFA) followed by HCI assay to evaluate the percentage of EBOV-GP expressing cells. Diazachrysene derivatives were tested as water soluble hydrochloride salts, while naphthyridines were tested as free base forms (1.0 % DMSO/water).

Table 1. Inhibitory activity of naphthyridine derivatives against EBOV and their cytotoxicity in HeLa cells.

Compound	EBOV EC_{50} (μM)	EBOV EC_{90} (μM)	CC_{50} (μM)	SI
1 (ZS48)[31]	0.70	<5	>20	>28.5
	0.55[a]	1.36[a]	>20[a]	>36.5[a]
2 (ZSML08)	0.26	0.85	8	30
	0.21[a]	0.78[a]	2.4[a]	11.2[a]
3	not active	-	>25	-
4	0.78	4.73	>10	>13
5	~10	-	-	-
8	not active	-	-	-
9	~10	-	-	-
10	not active	-	-	-
11	2.87	13	>25	>8.7
12	~10	-	-	-
13	4.82	37.43	>10	>2
14	not active	-	-	-
15	14.11	62.6	>25	>1.8
16	2.24	9.9	>25	>11.2
19	0.79	4.85	>10	>12.6
20	0.60	3.50	>10	>16.7
21	3.53	6.74	7	2.0
22	~10	23.5	>10	>1
23	~10	20.5	>10	>1
CQ[21,b]	16	-	-	-

ACCEPTED MANUSCRIPT

Table 1: EC_{50} or EC_{90}, which is the effective concentration to achieve 50% or 90% infection inhibition respectively, and CC_{50} (50% cytotoxicity) was accomplished by running the dose response curve analysis in four replicates (n = 4). Selectivity index (SI) =CC_{50}/EC_{50}. HeLa cells were used for assays, unless noted otherwise. [a]HFF cells. [b]Vero cells.

Several bis-aminoalkyl naphthyridine derivatives (**4**, **13**, and **16**) were found active in this assay (Table 1) with compound **16** with morpholino substituents connected with four carbons to aromatic moiety among the most active anti-infectives with EC_{50} = 2.24 µM. Other bis-aminoalkyl derivatives, such as **4** and **13**, were also considerably active, with EC_{50} = 0.78 µM and 4.82 µM, respectively. Moreover, the low EC_{90} = 4.73 µM emphasized the possible high potency of **4** as anti-EBOV inhibitor. Interestingly, **11**, which possesses 7-chloroquinoline moiety as its side-chain (a feature of **CQ**) also has acceptably good in vitro activity with EC_{50} = 2.87 µM, contrary to the mono-aminoalkyl substituted naphthyridines (**5**, **8**, **9** and **10**) which appeared either completely inactive or possessed borderline activity in our screen.

Diazachrysene derivatives with dissimilar aminoalkyl substituents, **2**, **19** and **20** showed improved anti-EBOV activity (Table 1) as compared to their symmetrically substituted analogue **1** and related compounds[31] with EC_{50} = 0.26-0.79 µM, and they also retained the low level of cytotoxicity. The inhibitor **2**, EC_{50} = 0.26 µM, EC_{90} = 0.85 µM, appeared as one of the most potent EBOV inhibitors known.[16,41,42] The most active new compound **2**, as well as our preceding derivative **1**, were further tested in a primary cell-based assay, in HFF cells. The activity proved to be consistent with HeLa based assay results.

Symmetrically substituted diazachrysene derivatives **21**, **22** and **23** showed no improved activity and were rather in-line with our previous results.[31]

Pharmacokinetic analysis and physicochemical properties

The in vitro ADME profile for compounds **2**, **4**, and **13** (Table 2) was encouraging. Both naphthyridines **4** and **13**, as well as the diazachrysene **2**, showed good plasma stability (60 or >85% remaining after 1 h), adequate solubility at pH 7.4 (>50 □g/mL), low to moderate CYP inhibition, and high mouse and human microsomal stability. Compound **2**, the most potent inhibitor, was further shown to be highly permeable in an MDCK permeability assay.

Table 2. ADMET parameters for **2**, **4**, and **13**.[43]

Parameter tested	**2**	**4**	**13**
Plasma stability, 1h, 37 °C (%)[a]	60	>85	>85
Solubility, pH 7.4 (μg/mL)[b]	>50	>50	>50
CYP3A4 / BQ inhibition (μM)[c]	>10	>10	>10
CYP3A4 / DBF inhibition (μM)[c]	>10	>10	>10
CYP3A4 / BFC inhibition (μM)[c]	>10	>10	>10
CYP2D6 / AMMC inhibition (μM)[c]	>10	8.0	>10
CYP2C19 / CEC inhibition (μM)[c]	>10	3.6	>10
Clearance mouse/human (μL/min/mg)[d]	22.3/32.9	32.9/<23	<23/<23

Microsomal $t_{1/2}$ mouse / human (min)[d]	62.1/42.1	42/>60	>60/>60
Permeability A→B (10^{-6} cm/s)[e]	39.3	-	-
Permeability B→A (10^{-6} cm/s)[e]	43.2	-	-

[a]Plasma stability (percent remaining after 1 hour), determined following incubation for 1 hour at 37 °C. [b]Compound solubility, determined using laser nephelometry to measure light scattering, performed in triplicate. [c]The IC_{50} values for CYP inhibition, determined from the net fluorescent signal from incubation at 37°C for a set time with an active cytochrome P450 enzyme and a fluorescent probe substrate. [d]Clearance in mouse and human models, substrate depletion experiments were performed by incubating test compound with liver microsomes for 1 hour at 37 °C; in this test $t_{1/2}$>30 min is considered good. [e]Apparent permeability (P_{APP}) of compounds determined with Madin Darby Canine Kidney (MDCK) Cell line; A→B apical to basolateral membrane movement; B→A basolateral to apical membrane movement; three biological replicates.

In order to assess the efficacy of diazachrysene transport, the interactions of **2** and **1** with HSA and AGP proteins, respectively, have been evaluated utilizing changes in fluorescence spectra of proteins upon addition of increasing amounts of each compound (see Supporting Information 1). The binding constants (K_{SV}) were (6.12±0.20) × 10^4 M^{-1} for AGP and (8.85±0.30) × 10^4 M^{-1} for HSA (for **2**); and (8.12±0.07) × 10^4 M^{-1} for AGP and (1.13±0.04) × 10^5 M^{-1} for HSA (for **1**).[44,45]

Furthermore, during in vivo tolerability evaluation of **2** in healthy mice (vide infra) mouse serum was collected and analyzed for total compound levels, and possible metabolites thereof.[46] Total concentration of compound **2** was detected in serum (0.35-1.20 µM) 24 h after last 20 mg/kg dose was administered, as presented in Figure 3. The detected concentration is conveniently in the range of the compound's EC_{90} value (0.85 µM), exceeding the EC_{50} value (0.26 µM HeLa; 0.21 µM HFF) and is significantly lower than the CC_{50} value in HeLa, and HFF

cell assays and the LC_{50} value of 18.9 µM (zebrafish assay, see Supporting Information 1). Moreover, this serum concentration relative to EC_{50} is similar to that for our diazachrysene compound **1** (0.46-1.03 µM; Supporting Information 1) which was efficacious in a mouse model of EBOV infection.

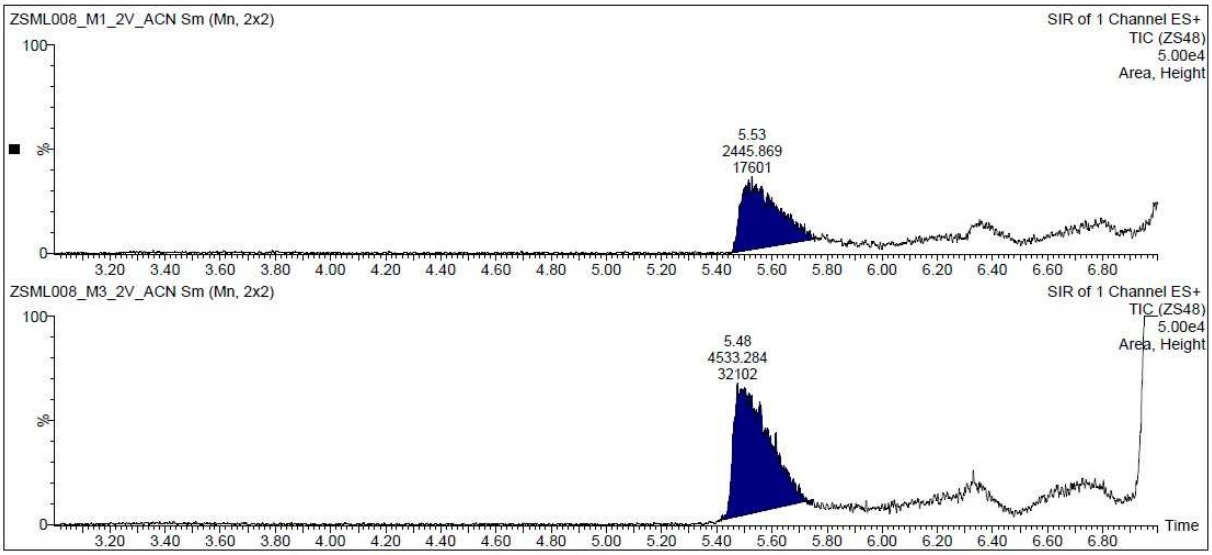

Figure 3. Chromatograms of quantification of free **2 (ZSML08)** levels in mouse serum. Samples from two mice treated with 20 mg/kg/day of **2 (ZSML08)** were taken 24 hours after the last dose and prepared as described in Supporting Information 1. Chromatograms were obtained using UHPLC/MS. No products of reduction (M+2), oxygenation (M+16), dehydrogenation (M-2), bis-oxygenation (M+32) or of any combination thereof were detected.

The ability of a compound to be protonated inside of the endosome is critical for the CAD mechanism. Therefore, acidity constants for three compounds selected for in vivo screening (**2**,

4, **13**) were experimentally determined by potentiometric titration in four replicates as presented in Table 3 and Figure 4 (conjugated acids, Supporting Information 1), as well as for **CQ** and **1**, for comparison. This allowed the calculation of the net charge for the compounds at physiological and lysosomal pH (Table 3). Furthermore, the distribution coefficients at pH=7.3±0.1 were calculated using ACD/Labs software.

Table 3. Experimental acidity constants of selected compounds and calculated distribution coefficients.

Compound	pKa side chain 1[a]	pKa side chain 2[a]	pKa core 1[b]	pKa core 2[b]	Net charge at pH 7.35[c]	Net charge at pH 5.0[c]	$clogD_{pH=7.3}$[d]
1[17]	5.96	5.24	7.35	4.37	0.54	2.72	2.71
2	6.65	5.60	7.70	4.56	0.87	3.04	2.53
4	10.81	8.41	5.72	/	1.94	2.84	1.36
13	10.97	8.50	5.51	/	1.95	2.76	-0.18
CQ	9.18	/	7.45	/	1.54	1.99	1.53

[a]pKa values of alkylamino side-chains. [b]pKa values of one or two aromatic nitrogens at the core. [c]Total degree of protonation (net charge) at (physiological) pH = 7.35 and pH = 5.0 (lysosome), respectively, calculated from pKa values (approximating the ionic strength of solution to zero). [d]Calculated distribution coefficient at pH 7.3 using ACD/Labs Release 12.0.[47]

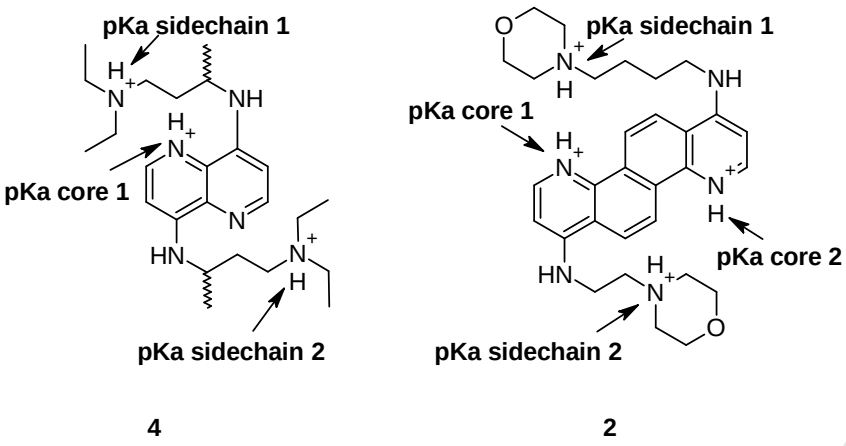

Figure 4. Sites of protonation from pKa determination experiment.

The pKa measurement results showed that naphthyridine derivatives **4** and **13** are more basic than diazachrysenes **2** and **1**, having two times higher net charge at physiological pH. This fully corresponds to their computed clogD values which are lower than the values of diazachrysene derivatives. The charge at physiological pH deserves a few comments: diazachrysenes, **2** and **1**, are less than monoprotonated at pH 7.35 and charge distribution sits ca. 79-93 % at core nitrogen and the rest stays on morpholine nitrogens (Supporting Information 1).[48,49] Therefore, the positive charge delocalization across the aromatic diazachrysene core should ease the plasma transport and passage across membranes of **1** and **2** over **4** and **13** (both possessing +2 localized charge at side-chain nitrogens) as in vivo results would suggest. On the other hand, the charge at pH 5.0 (lysosomal compartments) is very similar for all new compounds, being ~3.0; therefore, the higher degree of protonation is expected to prevent the compound from leaving the endosomal compartment once inside (vide infra).[50]

Toxicity profiling

The most promising EBOV inhibitor **2**, and **1** and **CQ** for comparison, were thoroughly investigated for toxicity in vivo (mortality, teratogenicity, cardiotoxicity, hepatotoxicity and myelosuppression) using zebrafish embryos (Figure 5).

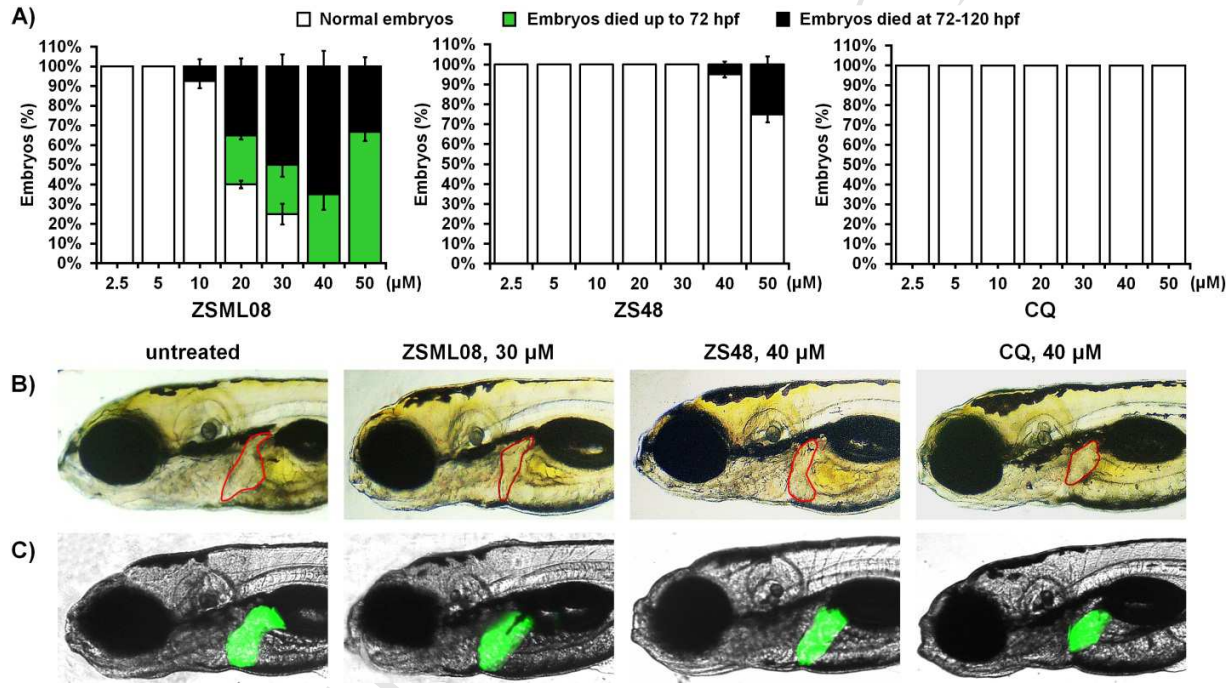

Figure 5. A. The results of toxicity assay on zebrafish embryos at 120 h hours post fertilization (hpf) exposed to antiviral drugs **2 (ZSML08)**, **1 (ZS48)** and **CQ**, expressed as the LC_{50} (μM). B. Morphology of wild type (wt) zebrafish embryos after the treatments with 30 μM of **2 (ZSML08),** 40 μM of **1 (ZS48)** and 40 μM of **CQ**. The embryonic liver is indicated with a red curved area. C. In vivo imaging of the liver morphology of *Tg*(*l-fabp*:EGFP) zebrafish larvae treated with **2 (ZSML08)** and **1 (ZS48)** confirming the lack of their hepatotoxicity upon applied doses contrary to **CQ**. For details see Supporting Information 1.

The antivirals **1** and **2** exhibited a dose-dependent mortality and did not induce any appearance of teratogenic (developmental) malformations in the surviving embryos (Figure 5; Supporting Information 1). As the cardiotoxicity and the liver toxicity are the most common drawbacks of the drugs approved for human use, diazachrysenes **1** and **2** were checked for the above toxic effects every day within 72-120 hours post fertilization (hpf). The obtained results showed no cardiotoxic effects in any of the surviving embryos, such as the appearance of pericardial edema (Figure 5B) and the disturbed heartbeat rate (data not shown).

To address the possible hepatotoxicity of selected diazachrysenes, we explored their effect on the liver development (applying compounds at 6 hpf when the liver has not yet been formed) and function (applying compounds at 72 hpf when the liver is fully functional) using the transgenic *Tg*(*l-fabp*:EGFP) zebrafish embryos with fluorescently labeled liver. The hepatotoxicity was evaluated at 120 hpf old embryos, using the liver area index (the ratio of liver area and lateral body area) that proved to accurately represents the liver damages.[51] As shown in Figure 5C, the antivirals **2** and **1** did not change the liver area index nor its fluorescence at any tested dose up to 30 μM and 40 μM, respectively, irrespective to the time of addition (Figure 5B, 5C, Supporting Information 1), thus clearly demonstrating no liver toxicity even at concentrations 73 times higher than cell based activity EC_{50} (for **2**) and 103 times higher (for **1**). On the contrary, **CQ** significantly reduced both the liver area index ($P < 0.05$) and fluorescence at ≥ 30 μM if administered at 6 hpf (Figure 5B, C), and at ≥ 80 μM when applied at 72 hpf (Supporting Information 1).

Since myelosuppression is also one of the adverse side effects of many clinically used drugs, the antivirals **1** and **2** were examined for toxicity in vivo towards neutrophils. To address this potential issue, we used the transgenic *Tg*(*mpx*:GFP) zebrafish embryos with fluorescently

labeled neutrophils, thus enabling direct visualization of applied compounds on the neutrophil genesis and occurrence. Obtained results revealed that **1** and **2** exerted no myelotoxic effect at any tested concentration up to 20 µM and 40 µM respectively, as determined by the whole embryos fluorescence (Figure 6). **CQ** appeared to be myelotoxic and markedly reduced the neutrophil occurrence at the doses ≥ 80 µM (Figure 6).

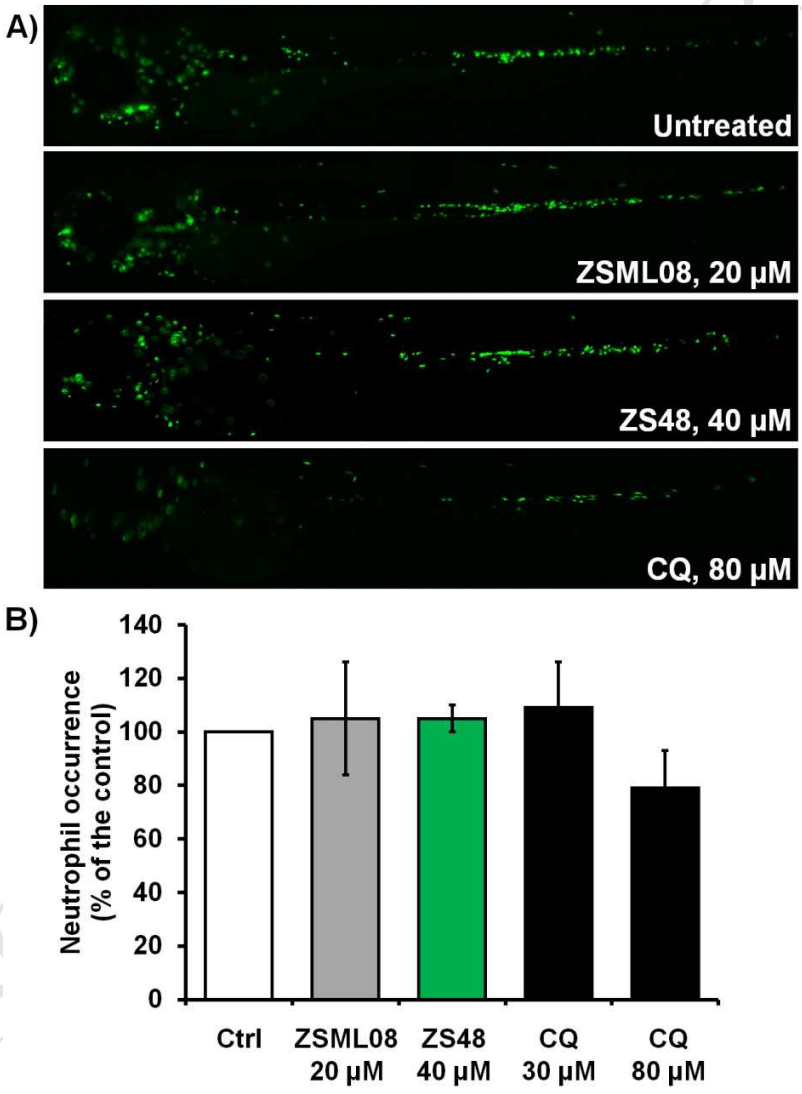

Figure 6. The effect of **2 (ZSML08)** and **1 (ZS48)** on the neutrophil population assessed in *Tg(mpx:GFP)* zebrafish embryos with GFP-labeled neutrophils at 72 hpf. Neutrophil fluorescence (A) and occurrence (B) upon the treatment with **2 (ZSML08)**, **1 (ZS48)**, and **CQ**.

To address the therapeutic potential of the explored compound, the toxicity was evaluated by determination of the lethal concentration (LC_{50}, Supporting Information 1), defined as the treatment concentration resulting in 50% mortality of embryos over a period of 120 hpf. The obtained results reveal a very good therapeutic potential of both diazachrysenes that showed a low overall toxicity with the $LC_{50(\mathbf{2\ (ZSML08)})}$ = 18.9 µM and $LC_{50(\mathbf{1\ (ZS48)})}$ = 72.1 µM. The observed toxicity is ~70-100 times lower than their respective inhibitory activity against EBOV observed in HeLa (HFF) cells, Table 1.

Tolerability studies in mice

Six healthy mice were subjected to seven daily doses of **2** (20 mg/kg, a dose twice as high as the one used in the EBOV challenge test; i.p. administration, c.f. Supporting Information 1). The mice were then observed twice daily for behavior and appearance for a total of 28 days after the last administered dose. No overt manifestations of acute toxicity were observed.

Compound 2 Protected Mice from EBOV

Based on the above potency, cellular toxicity, ADME, tolerability and PK properties, results, the two most potent inhibitors with minimal cytotoxicity, the compounds **2** and **4**, were further

evaluated for in vivo efficacy in a mouse model of EBOV infection[52] using three different doses of 10, 5 or 1 mg/kg (Figure 7). This mouse model has been often used for evaluating different antivirals.[20,27,41,53-55][53,54,55] A third compound, **13**, a less active homologue of **4**, was also chosen for comparison**.** Compound **2** showed a dose dependent protection with 100% protection at a dose of 10 mg/kg and 50% protection at lower doses of 5 mg/kg and 1 mg/kg (Figure 7A). Although uniform mice lethality was not observed in the vehicle treated control group infected with mouse adapted Ebola virus, a statistically significant ($p = 0.0013$) increase in survival was observed in the **2 (ZSML08)** (10 mg/kg) treated group compared to control group. Furthermore, minimal weight loss of the surviving mice was observed (Figure 7B). There was also 40% survival with **4** at its highest dose of 10 mg/kg (Figure 7C-D). These in vivo protection data corroborated with the compound's anti-viral activity derived from cell based assay (Table 1) with compounds potency following **2 (ZSML08)** > **4 (ZS103)** > **13 (ZS102)**.

ACCEPTED MANUSCRIPT

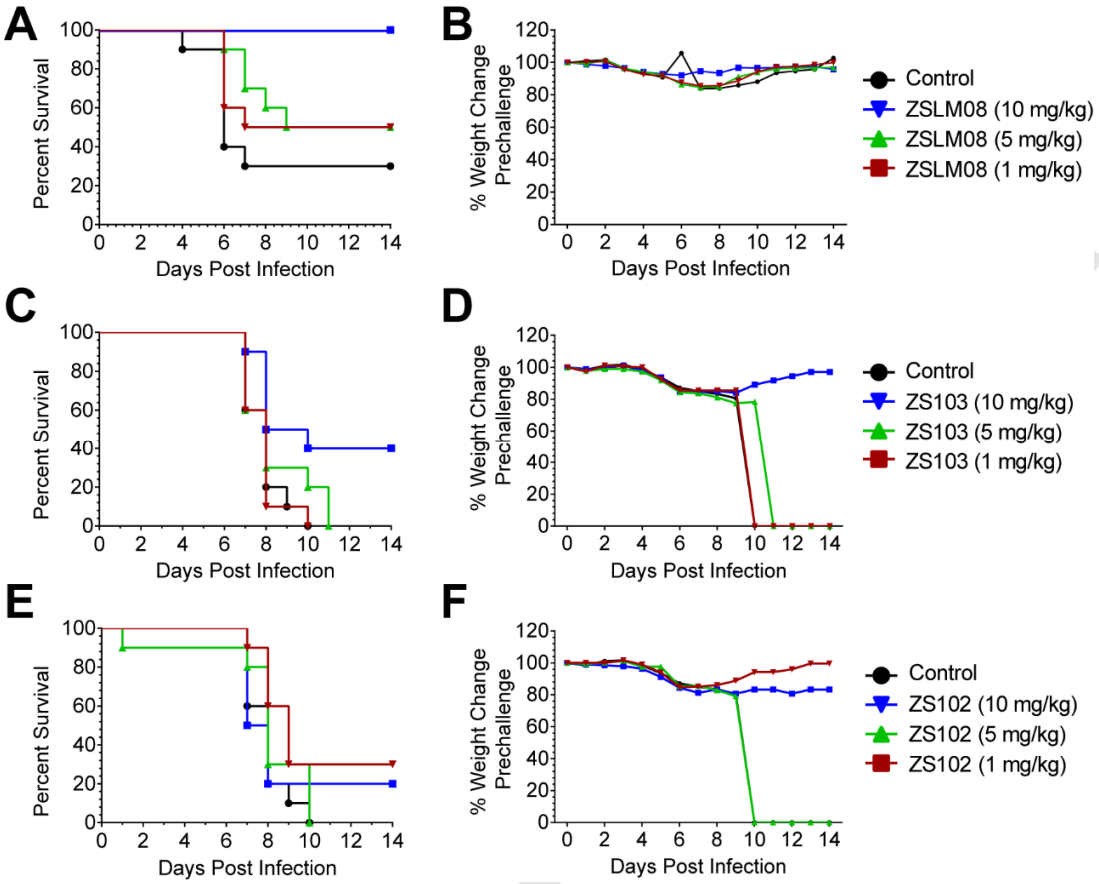

Figure 7. The compound **2 (ZSML08)** conferred most protection in mice from EBOV challenge. Mice (n = 10 mice/group) were treated with indicated concentrations of the compounds at 2 h prior to challenge with 1000 plaque forming units (PFU) of mouse-adapted EBOV. Treatment was continued daily for six days. The percent survival curves and the corresponding percent mean body weight change relative to day 0 (just prior to treatment or challenge) with **2 (ZSML08)** (A-B), **13 (ZS102)** (C-D) and **4 (ZS103)** (E-F) during the 14 days period of study. The P values were evaluated using log-rank test to compare survival rate with the control group. **2 (ZSML08)** p = 0.0013 (10 mg/kg); **19 (ZS103)**, p = 0.017 (10 mg/kg); **13 (ZS102)** p = 0.03 (1 mg/kg).

Investigation on the mechanism of action of diazachrysenes

Compounds 1 and 2 Blocked Viral Entry

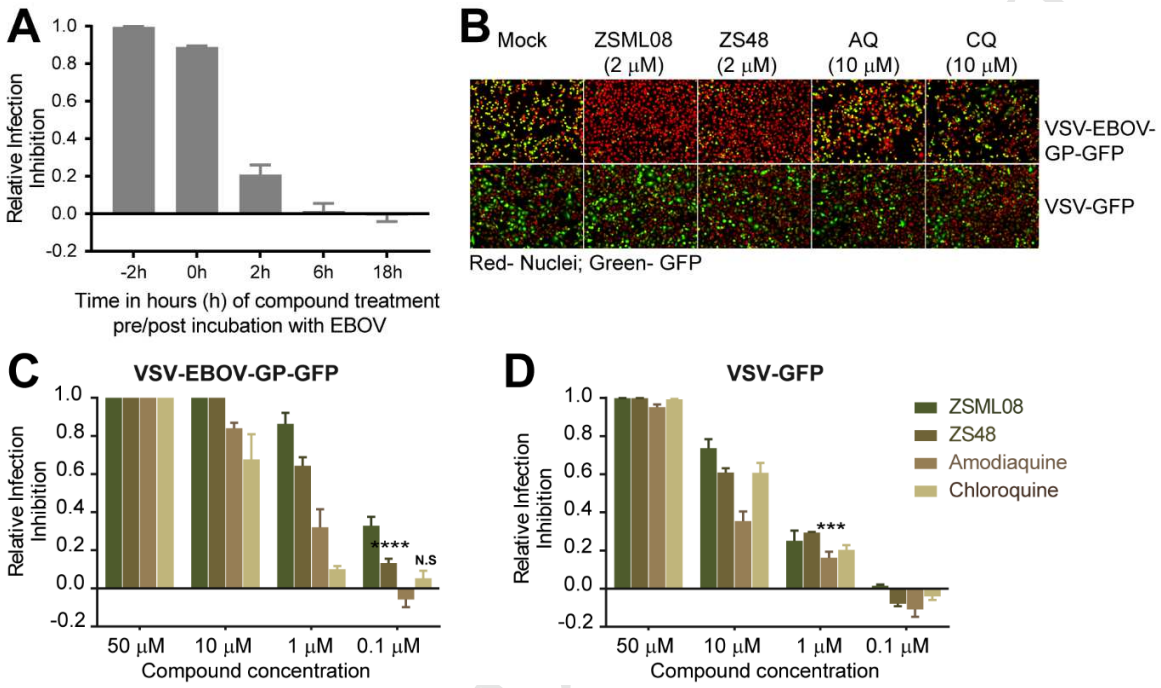

Figure 8. 1 (ZS48) and **2 (ZSML08)** target viral entry. (A) Time of Compound Addition assay (TCA) in which cells were untreated (mock) or treated with **2 (ZSML08)** (at 2 μM) at 2 h prior to infection (-2 h), or concurrent with virus infection (0 h), or at various time points post-incubation with EBOV (MOI=10 for 24 h), followed by immunofluorescence analysis (IFA) and HCI assay to determine the percentage of GP expressing cells. The infections at each time point were normalized with mock treated cells to determine the infection inhibition. (B) GFP expression by HeLa cells, which were pre-treated at 2 h with the indicated compounds followed by infection with rVSV-EBOV-GP-GFP or VSV-GFP viruses for 8 h and 6 h respectively. Cells were visualized by staining with Cell MaskDeep Red. (C-D) Same as in B but cells were either untreated (mock) or treated with indicated concentrations of the various compounds and infected

with rVSV-EBOV-GP-GFP (C) or VSV-GFP (D). Relative infection inhibition for each compound treatment was determined by normalizing percentage of GFP expressing cells with mock treated cells and subtracting the result with 1. Data is represented as mean ±SD of three replicates and is representative of three independent experiments. P values were evaluated by multiple t tests. N.S is not significant and ***, P<0.0001

CADs are known to target EBOV entry by modifying the internal milieu of LE/Ly, such that viral membrane is unable to fuse with host lysosomal limiting membrane.[19,56] Thus, we first examined if **1 (ZS48)** and **2 (ZSML08)** targeted viral entry by Time of Compound Addition (TCA) assay. As shown in Figure 8A, compound treatment prior to infection (-2 h) or at the time of infection (0 h) was necessary for its antiviral activity. Treating cells with the compound at 2 h after incubating with virus, by when the virus already entered cells, had no effect on virus infection.[57]

We next checked if defects in viral entry were indeed specifically related to changes in the LE/Ly without influencing early endosomes or other early entry events. To address this question, we used recombinant vesicular stomatitis virus (rVSV) that expressed green florescent protein (GFP) and either expressed its own GP (VSV-GP) or pseudotyped to express EBOV-GP (VSV-EBOV-GP) in the place of VSV-GP.[58] EBOV-GP trafficking to functional LE/Ly compartments is critical for its fusion competency, whereas VSV-GP trafficking to the early endosomal compartments is sufficient to make it fusion-competent.[59] Thus, if the compounds were modulating LE/Ly then their antiviral effects would be more pronounced in VSV infection regulated by EBOV-GP rather than VSV-GP. As shown in Figure 8 (B-D) even at 0.1 µM

concentration, **1** and **2** inhibited rVSV-EBOV-GP but had no effect on rVSV-GFP infection. At higher concentrations compounds inhibited VSV infection irrespective of the entry mediated by VSV-GP or EBOV-GP but were much more sensitive to entry by latter. Two controls, **AQ** and **CQ**, were also shown to inhibit EBOV entry albeit to a lesser extent.[18,28,60] At higher concentrations (50 µM) at which compounds were all cytopathic (Figure 8C-D), all compounds inhibited VSV infection. Collectively, these data confirmed that **1** and **2** targeted viral entry mostly by modulating LE/Ly functions and were significantly more potent when compared to the other structurally related CADs such as **CQ** and **AQ**.

Antivirals 1 and 2 are Lysosomotropic and Modify Acidic Compartments

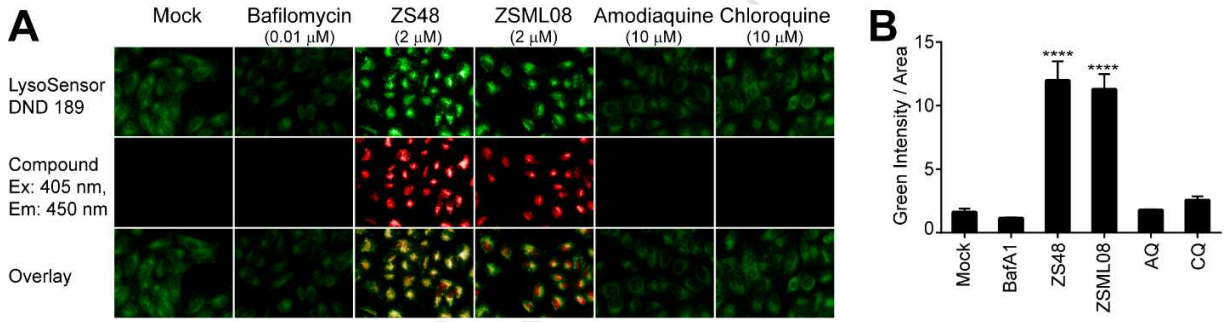

Figure 9. Compounds **1 (ZS48)**/ **2 (ZSML08)** are lysosomotropic. HeLa cells were untreated (mock) or treated with Bafilomycin A1 (BafA1) at 0.01 µM, **1 (ZS48)** at 2 µM, **2 (ZSML08)** at 2 µM, **AQ** at 10 µM and **CQ** at 10 µM for an hour followed by treatment with Lysosensor DND 189 for 10 min. (A) Cells were washed and then imaged at an excitation/emission of 443/505 nm and 405/450 nm for detecting Lysosensor dye and the tested compounds, respectively. (B) The intensity/area of the fluorescence emitted by the Lysosensor dye from the collected images as in A was further evaluated using image analysis software (Columbus). Each data point is mean ± SD of a replicate of 8 wells of a 96 well plate with approximately 3000 cells per well and is

representative of three independent experiments. P value was evaluated by One Way Anova analysis. ****, $P < 0.0001$.

CADs freely diffuse into cells but once inside an acidic compartment they become protonated and remain trapped. The ensuing physiological and morphological changes in the LE/Ly can make the virus fusion incompetent. The acidic pH of LE/Ly is also necessary for converting EBOV-GP to the cleaved fusogenic form that is essential for viral entry.[61] Thus, we examined **1 (ZS48)** and **2 (ZSML08)** effects on the morphology and pH changes of LE/Ly by live cell microscopy, using commercially available fluorescent reporter, LysoSensor DND 189, which localizes to acidic compartments, and exhibits pH dependent increase in fluorescence intensity upon acidification. HeLa cells were pre-treated with the compounds for 1 h prior to imaging cells with LysoSensor. Compounds **1** and **2** were also fluorescent that allowed their visualization at an excitation (Ex. 405) and emission (Em. 450). There was no fluorescence detected by the compound alone under the Ex/Em conditions used for visualizing LysoSensor (data not shown). As shown in Figure 9A, antivirals **1** and **2** strongly co-localized with LysoSensor suggesting that these compounds freely diffused into cells, but once inside the acid compartments, they became heavily protonated (~ZSH_3^{3+}, Table 3, Figure 4) and trapped. Furthermore, **1** and **2** induced the clustering of LE/Ly at a high density, unlike in mock treated cells, in which they were fewer and showed dispersed distribution throughout the cytoplasm (Figure 9, A-B). Surprisingly, there was also sharp increase in florescence intensity of the acid compartments, thus ruling out the possibility of neutralizing or alkalizing of LE/Ly due to compound protonation. LysoSensor 189 sharply drops its florescence intensity by both, decreasing pH from 4 to 0.5 or by increasing pH from 4 to 9.[62] The plausible explanation for the increase in intensity appears to be due to an increase in uptake of LysoSensor by the expanding LE/Ly (vide infra). The additional CAD

controls, **CQ** and **AQ** showed a minor increase in fluorescence intensity when compared to mock treated cells (Figure 10B) but no other changes were noted. As expected, control Bafilomycin A1 (BafA1) treatment, an inhibitor of vacuolar H^+ ATPase that regulates low acidic pH in the lysosomal lumen, reduced the fluorescence intensity.[63]

We next examined if **1 (ZS48)** and **2 (ZSML08)** expanded the acidic compartments using lysosomotropic weak base Acridine Orange (AO). AO binds to DNA and RNA as a monomer and emits fluorescence in green channel. However, uptake of AO and its retention in protonated (AOH^+) form in the acid compartments, increases its local concentration several fold causing AOH^+ oligomerization and shifting its florescence spectra from green to red. Furthermore, increase in the intensity of red fluorescence is proportional to the increase in concentration of AOH^+ in LE/Ly.[64] No fluorescence was detected by the compound alone under the Ex/Em conditions used for visualizing AO (data not shown).

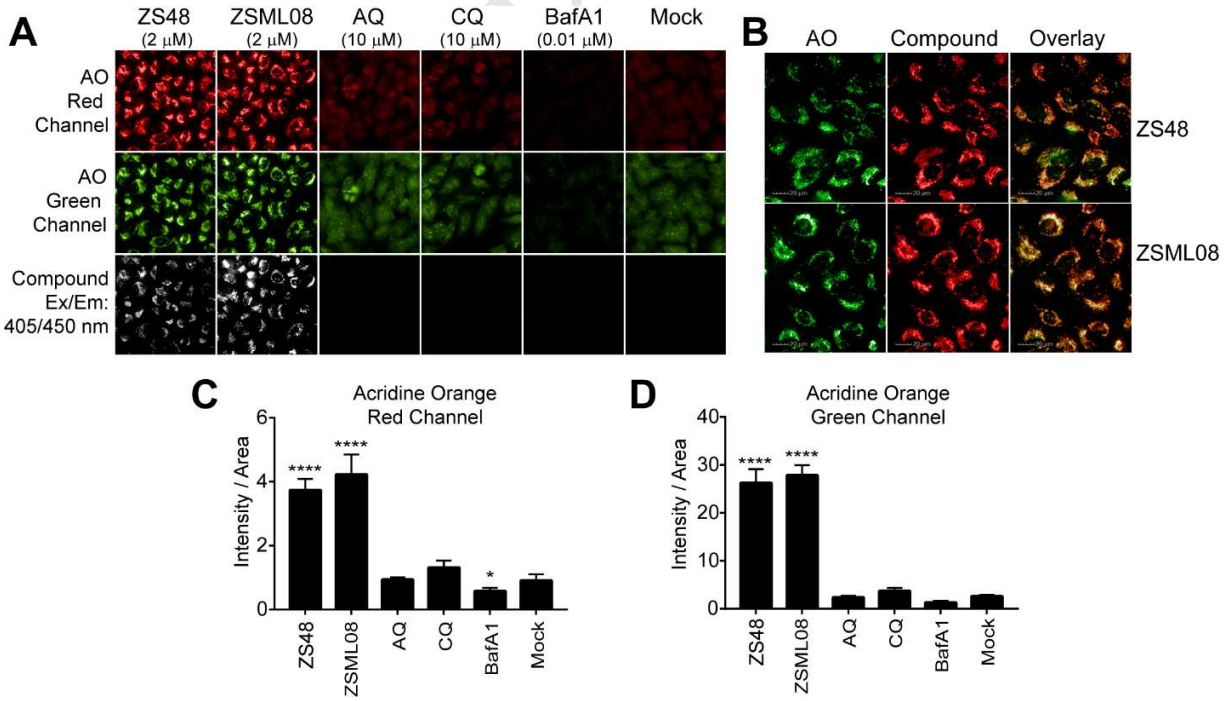

Figure 10. Compounds **1 (ZS48)** and **2 (ZSML08)** induce expansion of acidic compartments. HeLa cells were pre-treated for 2 h with the indicated compounds followed by incubation with Acridine Orange (AO) for 30 min. Cells were washed prior to imaging at the indicated wavelengths. (A) The localization of AO and the **1 (ZS48)**/ **2 (ZSML08)** compounds. In (B) images were enlarged to demonstrate co-localization between AO and compounds **1 (ZS48)**/ **2 (ZSML08)**. In C and D, the total intensity and the average area of florescence emitted by AO were evaluated by HCI assay. Each data point is mean ± SD of a replicate of eight wells of a 96 well plate with approximately 3000 cells per well and is representative of three independent experiments. P value was evaluated by One Way Anova analysis. ****, $P < 0.0001$. *, $P < 0.05$.

As shown in Figure 10, treatment with **1 (ZS48)** and **2 (ZSML08)** had a profound effect on both the intensity and distribution of AO when compared to mock treated cells. First, there was a robust increase in the red florescence of AO suggesting an expansion of the acidic compartments (Figure 10A). Second, compounds strongly co-localized with AO in the acidic compartments (Figure 10B) which validated our previous observations of the lysosomotropism of **1** and **2**. Third, a majority of AO localized to the vesicular compartments that showed dense clustering at the perinuclear region while there was very little green signal (480 nm emission) in the cytoplasm from monomeric AO binding to DNA/RNA. It appears that the expanding LE/Ly compartments retained their acidity which culminated in the uptake and retention of a majority of AOH^+. A small increase in the concentration of lysosomes at the juxtanuclear regions was also evident in **CQ** and **AQ** treated cells. As expected, the control BafA1 decreased AO red signal in the LE/Ly. Taken together, **1** and **2** are lysomotropic, induced expansion and dense clustering of

LE/Ly without increasing vacuolar pH. We next examined how the inhibitors influence lysosome functions that directly impact EBOV entry.

Antivirals 1 and 2 Inhibited Cathepsin B Activity

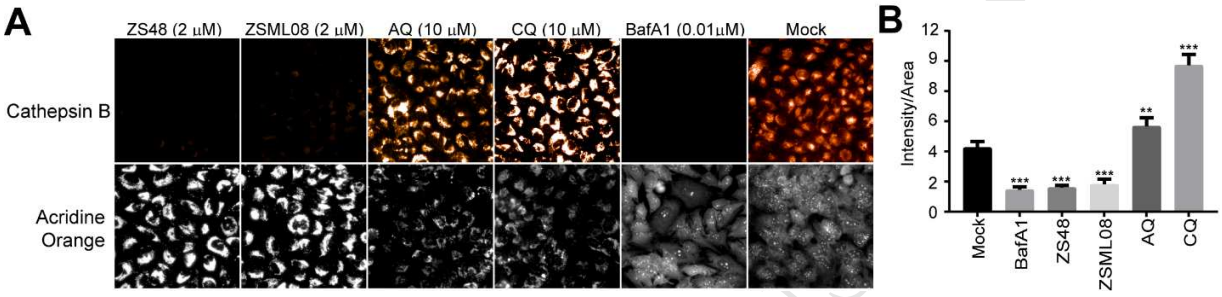

Figure 11. Compounds **1 (ZS48)**/**2 (ZSML08)** inhibited Cathepsin B activity. HeLa cells were treated with the indicated compounds for 12 h followed by treatment with Magic Red reagent or with AO for 10 min and 30 min, respectively. (A) Cells were washed and then imaged at an Ex/Em of 590/630 or 520/560 to detect florescence emitted by the Magic Red or AO, respectively. Increase in florescence by Magic Red is indicative of cathepsin B activity. (B) The total intensity and the average area of florescence emitted by Magic Red from the images collected were evaluated by HCA. Each data point is mean ± SD of a replicate of eight wells of a 96 well plate with approximately 3000 cells per well and is representative of three independent experiments. P value was evaluated by One Way Anova analysis. ***, $P < 0.001$. **, $P < 0.01$.

EBOV-GP cleavage by Cat-B and L, which reside in the LE/Ly, are critical for generating fusion competent virus. **AQ** and **CQ** inhibition of EBOV entry was previously attributed to their ability to block cathepsin's activity.[65] We examined if the same applies to **1 (ZS48)** and **2 (ZSML08)**. To achieve this, we used a peptide reporter which freely diffuses into all

compartments of the cells and emits red fluorescence upon cleavage by specific cathepsin. HeLa cells were treated with **1** and **2** for 12 h and then incubated with the peptide reporter for 1 h following which cells were washed and imaged.

As shown in Figure 11 (A-B), in cells treated with **1** and **2** there was a marked decrease in cathepsin B activity when compared to mock treated controls. We also observed a significant *enhancement* in the reporter activity in **AQ** and **CQ** treated cells contradicting a previous report.[65] BafA1 treatment, as expected, showed a significant decrease in cathepsin B reporter activity. Similar observations were made at lower duration of treatment (6 h) and with Cat-L reporter (data not shown), thus leading to our conclusion that **1** and **2** disrupted cathepsins activity.

Antivirals 1 and 2 Blocked Lysosome Fusion with Autophagosome

Some CADs including **CQ** and **AQ** block proper maturation of the lysosomes by disrupting lysosome's ability to fuse with the cargo containing vesicles including NPC1 expressing LE or autophagosomes.[66,67] These defects could potentially prevent the EBOV trafficking to the NPC1 expressing LE for viral entry. Thus, we examined the autophagosome fusion with lysosome using LC3 marker. LC3-I which is cytosolic, is converted into the membrane-bound form LC3-II as autophagy progresses, and specifically localizes on the autophagosome membrane. The autophagosome subsequently fuses with the lysosome to form the autolysosome. Defects in lysosome-autophagosome fusion will induce accumulation of LC3-II clusters.

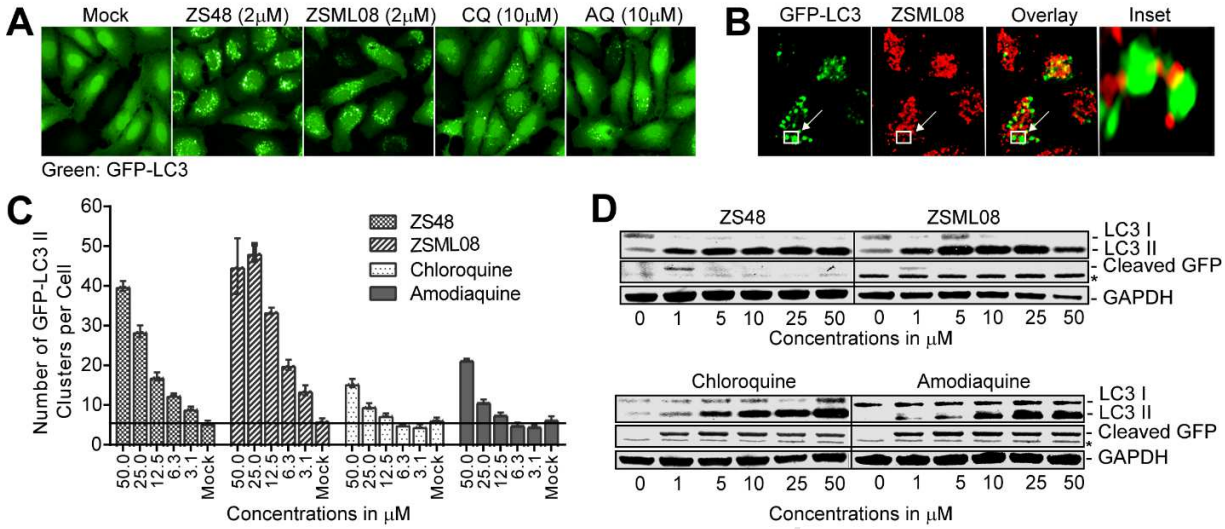

Figure 12. Compounds **1 (ZS48)** and **2 (ZSML08)** blocked autophagy. (A) HeLa cells stably expressing GFP-LC3 were treated with the indicated compounds for 4 hours followed by live cell imaging to detect GFP clustering. (B) Confocal images at higher magnification as in (A) to visualize the spatial distribution of **1 (ZS48)**/**2 (ZSML08)** loaded vesicles and the GFP-LC3-II clusters. Note that GFP clusters and **1 (ZS48)**/**2 (ZSML08)** loaded vesicles either did not co-localize or in some instances were adjacent to each other with partial overlap at the peripheral edges. The white box in the images is enlarged in the inset. (C) HeLa cells as in (A) were treated with indicated concentrations of the compounds for 4 h, followed by image captures. The images were analyzed to determine the total number of GFP clusters/per cell. Each data point is mean ± SD derived from 8 well replicate of a 96 well plate with approximately 500 cells per well and is representative of three independent experiments. (D) Western blots of HeLa cellular lysates that were subjected to the indicated concentrations of compounds for 6 h. * indicates non-specific band.

We thus examined microscopically, LC3-II clusters in compound treated cells using a HeLa cell line that stably expressed GFP-LC3. As shown in Figure 12 (A-B), all four CADs, **1 (ZS48)**, **2 (ZSML08)**, **CQ** and **AQ** showed an increase in GFP-LC3-II clustering compared to mock treated cells although the number of GFP clusters per cell were significantly higher in **1** and **2** treated cells (Figure 12A). Furthermore, most of the GFP-LC3-II clusters did not co-localize with **1 / 2** loaded vesicles (Figure 12B), although in some instances they overlapped partially at the periphery, implying arrested fusion between the lysosome and autophagosome. These observations were further confirmed by Western blot analysis that showed an increase in the membrane bound LC3-II expression levels in a dose dependent manner (Figure 12D), with the increase in LC3-II clusters being more sensitive to **1 / 2** when compared to **CQ** and **AQ** treatments. Lastly, a clear difference was noted in the mechanism of autophagy inhibition between **1 / 2** and **CQ**/**AQ** when the levels of cleaved GFP were compared (Figure 12D, look at cleaved GFP levels). The luminal facing GFP-LC3-II in the autolysosome undergoes degradation in two steps. First GFP is cleaved followed by its degradation. In agreement with previous studies at non-saturating concentrations of **CQ** (< 50 µM), lysosome functions were not completely inhibited thereby allowing accumulation of cleaved GFP levels (Figure 12D). However, **1** and **2** were much more sensitive and efficiently blocked GFP-LC3-II degradation mostly by blocking autolysosome formation. Collectively, these data imply fusion defects of the LE/Ly compartments with the autophagosomes and that antivirals **1** and **2** were many times more sensitive than **CQ**/**AQ**.

Antivirals 1 and 2 Induced Expansion of Vesicular Compartments

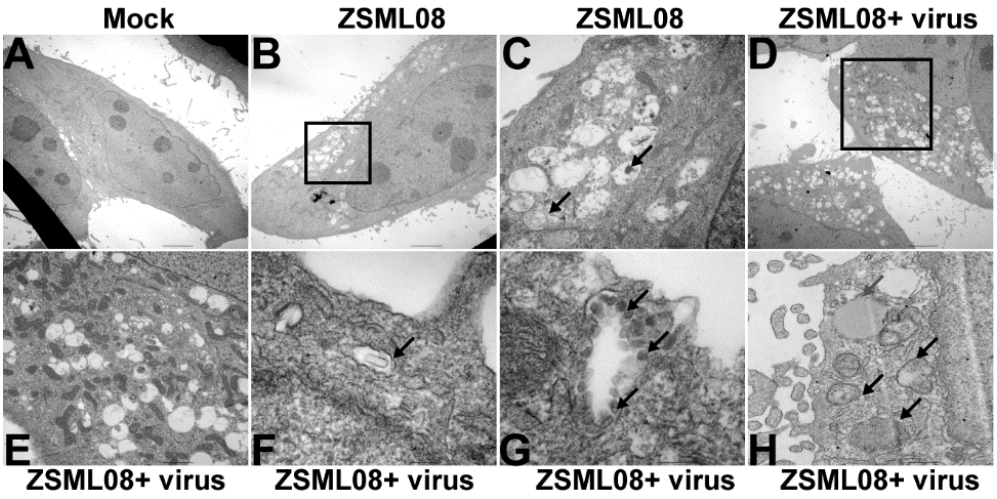

Figure 13. Electron microscopy images of **2 (ZSML08)** treated HeLa cells. Cells were mock treated (A) or pre-treated for 2 h with **2 (ZSML08)** prior to mock incubation (B-C) or incubation with rVSV-EBOV-GFP for 2 h (F) or 6 h (D, E, G-H) followed by processing samples to acquire images by transmission electron microscopy. Inset in B and D were enlarged to images in C and E respectively. Black arrows in C point to lamellar and large granules containing vesicles, in F point to the rod shaped VSV-EBOV like particles, in G point to multivesicles containing compartments, and in H mark the double membraned autophagosomes.

Lastly, we used electron microscopy to visualize how **2 (ZSML08)** modified EBOV trafficking and vesicle morphology in HeLa cells. Until this point we did not observe any differential activity between compound **1 (ZS48)** or **2 (ZSML08)** in modifying Lysosome functions and therefore we chose compound **2** which was most potent against EBOV and the main subject of this study for electron microscopy studies. To this end, HeLa cells were either mock treated or treated with compound **2** for 2 h and then were either left uninfected or infected with VSV-EBOV-GP-GFP virus for 2 h or 6 h. Cells treated with compound **2** irrespective of virus

infection showed a marked expansion in the number and volume of vesicular compartments when compared to mock treated cells (Figure 13 A-D). These vesicles accumulated lamellar structures, lipids, smaller vesicles and aggregates, implying defects in lysosome hydrolytic activities. Furthermore, at early stages of infection (at 2 h), accumulation of bullet shaped VSV-EBOV-GFP viral like particles in vesicular compartments were visible in **2** infected cells suggesting virus internalization (Figure 13F). In addition, several double membraned vesicles presumably autophagosomes were also observed (Figure 13H). Lastly, vesicle expansion was concentrated to one side of the nucleus further confirming our previous observations. Collectively, these data confirmed that diazachrysene **2** enhanced vesicle expansion, and modified lysosome functions.

Discussion

Here we present the preparation and antiviral activity examination of the new class of heterocyclics, 1,8-dialkylamino naphthyridines. Their structure was based on core reduction approach to remodel the diazachrysene core of our successful leads, e.g., **1** (**ZS48**).[31] In addition, in fine-tuning of **1** we succeeded to develop the unsymmetrically substituted class of diazachrysenes. All 18 synthesized compounds were screened in a HeLa/HFF cell-based assay for their anti-EBOV activity. New naphthyridine inhibitors **4, 13** and **16** were found active in low-micromolar range, however, our new, unsymmetrically substituted, diazachrysenes **2, 19** and **20**, proved to be the most active compounds in vitro with good CC_{50}/EC_{50} selectivity index (Table 1). The ADMET studies of three most promising derivatives (**2, 4** and **13**) exposed their very low to moderate CYP inhibition, which with good plasma stability, sufficient solubility and

low clearance give support to our approach to new and stable CADs. Further, the most active diazachrysene derivative **2**, and its congener **1**, were examined in zebrafish toxicity model appearing not to induce any teratogenic malformations in survived embryos, along with no signs of cardio- and hepatotoxicity, and expressed no myelotoxic effect at any tested concentration.

Naphthyridines **4**, **13**, and diazachrysene **2** were submitted to the EBOV challenge test in groups of ten mice per each compound using standard dosage regimen (once daily for 7 days). Derivative **2** manifested a dose-dependent increase in mice survival with the highest dose (10 mg/kg) resulting in 100% survival. Perhaps most importantly, during the entire duration of the in vivo studies, the respective mice groups retained their weight, which otherwise decreases in mice with EVD. Very few known small molecule EBOV inhibitors achieved full protection in mice, which points to successful fine-tuning of the hit structure **1**.[17] We speculate that the inferior activity of naphthyridine derivatives (survival: 40% and 20%) for **4** and **13** as compared to diazachrysene **2** could be correlated to their basic physicochemical properties, such as a higher positive net charge and lower distribution coefficient at physiological pH (vide supra). In addition, low concentration of diazachrysenes in serum, and determined K_{SV}, appear to ensure the compound's efficacy while maintaining safe (nontoxic) drug concentration (total **2**: 0.35-1.20 μM; vs. $LC_{50(2)}$ = 18.9 μM and total **1**: 0.46-1.03 μM vs. $LC_{50(1)}$ = 72.1 μM). The main transporter plasma proteins are HSA and AGP, which very often scavenge the intended drug from reaching the target, and our HSA and AGP measurements of diazachrysene **2** revealed the optimal drug binding and drug release (K_{SV} within 10^4 - 10^6 M^{-1}).[68-70][68,69,70]

As noted before, several of the FDA approved drugs with anti-EBOV activity belonged to the CAD group with EC_{50} values mostly in the range of 10 μM.[13,18-20,71-73][13,18,19,20,71,72,73] The compounds described in this study also possess CAD moiety and are lysosomotropic but are

much more potent with EC_{50} values in the range of 0.2 – 0.7 μM. This could be due to their fast kinetics of uptake and retention into the lysosomes and their ability to alter specific interactions within the lysosomal compartment that is essential for EBOV entry. As noted above, the pKa profile of diazachrysenes allows for a smaller and delocalized charge than many CADs at physiological pH, enabling them to pass across membranes more easily. This assumption is supported by MDCK-based assays that showed good permeability of **2** at physiological pH.

Typically, lysosomotropic compounds including **CQ** and **AQ**, were thought to disrupt the lysosome functions by raising its intra-luminal pH.[74] Lysosomes digest a variety of substrates derived from both cellular and extracellular origins via phagocytosis, endocytosis and autophagy degradation pathways. This is accomplished by the enclosed hydrolases, including proteases, nucleases, lipases, sulfatases or phosphatases, whose pH optima are usually low (pH 4.5–5). An increase in lysosomal pH, can block the hydrolytic activities leading to an accumulation of undigested substrates including lipids, protein aggregates and organelles etc. in the lysosomes. However, our data shows that compounds **1** and **2** including **CQ** and **AQ**, retained lysosome acidity, based on LysoSensor and Acridine Orange staining. Our data aligns with a more recent study which demonstrated that lysosomotropic compounds including **CQ**, although initially (within 30 min) increased lysosomal pH, those changes were transient and were quickly reversed (within 2-4 hours).[75] Few other studies too demonstrated that longer incubations of the lysosomotropic compounds in many different cell types did retain the acidic pH of the lysosome.[76] Thus, our data provides credence to the new observations that disruption in lysosomal functions by lysosomotropic compounds may not be driven by increasing pH.

The most striking observation was the rapid expansion of lysosomes by compounds **1** and **2** within an hour of treatment and at a low dose of 1 μM. Similar phenotype can be achieved by

CQ or few other lysosomotropic compounds, but only upon longer duration of treatment (>24 h) and that too at much higher doses (50-100 μM). Recently, Lu et al[75] demonstrated that lysosomal expansion by lysosomotropic compounds is regulated by the activation of coordinated lysosomal enhancement and regulation (CLEAR) network that controlled expression of multiple genes involved in lysosomal biogenesis and lysosome related functions.[75] Compound accumulation inside lysosomes was shown to trigger "lysosomal stress program" that lead to the translocation of transcription factor including TFEB and TFE3 into the nucleus, to activate genes regulating lysosomal functions via binding to the CLEAR elements in their promoters. Lysosomal stress also induced a reduction in mTORC1 activity and calcium signaling which activated the CLEAR network. These changes were described as lysosomal adaptations to counter the lysosomal stress. Future studies are required to address if the same holds true with compounds **1** and **2** and if these compounds can indeed disrupt calcium signaling and mTORC activities to induce the CLEAR pathway.

Despite rapid expansion of lysosomes by **1** and **2**, these changes did not necessarily activate lysosome functions. Instead and similar to other lysomotropic compounds, severe defects in hydrolytic activities of lysosomes were observed.[75] Our EM images, showed an accumulation of undigested material inside lysosomes including large aggregates of macromolecules, membranes, vesicles and lipids. However, unlike other lysomotropic compounds, cathepsins were also inactivated from early on by compounds **1** and **2** treatment, which could be due to leakage of cathepsins by alterations in lysosome membrane permeability. While early studies suggested that **CQ** and **AQ** inhibited cathepsins by increasing lysosomal pH, our data, and studies by Lu et al[75], show that compensatory lysosomal adaptions in response to lysosomal stress can actually enhance cathepsin's activity. Thus, the rapid expansion of lysosomal

compartments accompanied by inhibition of hydrolytic activities including inactivation of cathepsins might make these compounds more effective antivirals compared to other lysomotropic compounds.

Antivirals **1** and **2** blocked EBOV entry based on time of compound addition and pseudotyped viral entry assays. Furthermore, our electron microscopy studies support previous reports which show that CADs did not block viral endocytosis but blocked late stages of entry by preventing viral-host membrane fusion. In the case of compounds **1** and **2**, the late entry defects could due to defective proteolytic events (loss of cathepsin's activity) that result in fusion defective GP and or also due to impaired trafficking of the virions to NPC1 expressing LE/Ly compartments. The fusion between NPC1+ late endosomes and lysosomes plays an essential role in producing fusion competent EBOV-GP. Several cellular host factors such as Rabs, SNARE, homotypic fusion and protein sorting (HOPS)-tethering complex and Ca^{2+} ion that regulate the fusion between LE and lysosomes were shown to be essential regulators of EBOV entry.[25,77] The same factors also regulated fusion between lysosomes and autophagosomes.[78] Our studies show that compounds disrupted the ability of LE/Ly to undergo normal vesicle fusion by monitoring fusion between lysosomes and autophagosomes. Further studies are required to determine the direct fusion defects between the LE and Ly. Overall, our data suggest that **1** and **2** efficiently prevented trafficking of EBOV-GP to appropriate NPC1+ LE compartments or that these compartments were defective in the generation of a fusion competent EBOV-GP.

CADs are known to induce phospholipidosis, upon chronic treatment and at therapeutically relevant concentrations.[73,79] This phenotype is similar to the Niemann Pick type-C (NPC) disease, a lipid storage disease caused by lipid accumulation inside the vesicles. However, these potential side effects outweigh the benefits while treating Ebola viral disease. This is because

CADs in clinical use are well tolerated; phospholipidosis induced by CADs is not associated with the clinical outcome, the lipid accumulation is reversible upon the removal of CADs and the duration of treatment with CADs in Ebola viral disease is also short spanning few weeks to months. Overall the presented studies clearly emphasize the effectiveness of our antivirals of diazachrysene class, **1** and **2**, as prominent candidates for further structure-based development in quest for anti-Ebola drug.

CONCLUSION

Here, we report on the synthesis of the novel anti-EBOV pharmacophore with potential for further development – aminoalkyl substituted 1,4-naphthyridine. In addition, we optimized our diazachrysene-based compounds, as to obtain an EBOV inhibitor of high potency, compound **2** (EC_{50}/EC_{90} (HeLa) = 0.26 µM/0.85 µM). This compound also protects mice infected with EBOV with minimal weight fluctuation during the 14-day experiment. Zebrafish extensive tests revealed no teratogenicity, cardiotoxicity, hepatotoxicity and no myelotoxic effects of our diazachrysenes **1** and **2** which were well tolerated in healthy mice. We suggest that the observed tolerability and efficacy in mice could be correlated to low positive net charge of **1** and **2** at pH 7.35 that should ease the plasma transport (measured K_{SV} within 10^4 - 10^6 M^{-1}), good observed apparent permeability, and low total drug concentration in serum (ca. 1 µM). It was also found that our compounds specifically inhibit viral entry by interfering with cellular LE/Ly pathways thereby obstructing the prerequisite conditions for EBOV glycoprotein mediated viral ingress. Finally, we report on other beneficiary effects of our compounds, such as cathepsin inhibitory activity and certain traits that differ from other CADs, such as rapid expansion of endosomal volume.

Experimental Methods

Chemistry

Melting points were determined on a Boetius PMHK apparatus and were not corrected. IR spectra were taken on a Thermo-Scientific Nicolet 6700 FT-IR diamond crystal. ^{1}H and ^{13}C NMR spectra were recorded on a Varian Gemini-200 spectrometer (at 200 and 50 MHz, respectively), and a Bruker Ultrashield Advance III spectrometer (at 500 and 125 MHz, respectively) in the indicated solvent (*vide infra*) using TMS as the internal standard. Chemical shifts are expressed in ppm (δ) values and coupling constants (J) in Hz. ESI–MS (HRMS) spectra of the synthesized compounds were acquired on a Agilent Technologies 1200 Series instrument equipped with Zorbax Eclipse Plus C18 (100 × 2.1 mm i.d. 1.8 μm) column and DAD detector (190-450 nm) in combination with a 6210 Time-of-Flight LC/MS instrument in positive ion mode. The samples were dissolved in pure H_2O (HPLC grade). The selected values were as follows: capillary voltage 4 kV; gas temperature 350 °C; drying gas 12 L min-1; nebulizer pressure 45 psig; fragmentator voltage: 70 V. Lobar LichroPrep Si 60 (40-63 μm) or LichroPrep RP-18 columns coupled to a Waters RI 401 detector were used for preparative column chromatography. Mass spectral analyses were done using electrospray ionization in positive ion mode on a Surveyor separations module coupled to a ThermoFinnigan TSQ AM triple quadrupole mass spectrometer.

HPLC purity determination

Compounds **2-5**, **8-15** and **19-23** were analyzed for purity (HPLC) using a Waters 1525 HPLC dual pump system equipped with an Alltech Select degasser system and dual λ 2487 UV-VIS detector and using an Agilent 1200 HPLC system equipped with a Quat pump (G1311B), an injector (G1329B) 1260 ALS, TCC 1260 (G1316A) and a detector 1260 DAD VL+ (G1315C). HPLC analysis was performed using two of several different methods:

Method A: Octadecylsilica was used as the stationary phase (Zorbax Eclipse Plus C18 4.6 x 150 mm, 1.8 µ, S.N. USWKY01594). Compounds were dissolved in water. The final concentrations were ~ 1 mg/mL, and the injection volume was 3.0 µL for compounds **2** and **20** and 4.0 µL for compounds **19** and **21-23**. The eluent was made from the following solvents: 0.2% formic acid in water (A) and methanol (B). Wavelength = 254 nm.

Method B: Octadecylsilica was used as the stationary phase (Zorbax Eclipse Plus C18 4.6 x 150 mm, 1.8 µ, S.N. USWKY01594). Compounds were dissolved in water. The final concentrations were ~ 1 mg/mL, and the injection volume was 1.0 µL for compounds **2** and **20** and 4.0 µL for compounds **19** and **21-23**. The eluent was made from the following solvents: 0.2% formic acid in water (A) and acetonitrile (B). Wavelength = 254 nm.

Method C: Octadecylsilica was used as the stationary phase (Zorbax Eclipse Plus C18 4.6 x 150 mm, 1.8 µ, S.N. USWKY01594). Compounds were dissolved in methanol. The final concentrations were ~ 1 mg/mL, and the injection volume was 0.5 µL for compounds **9**, **10** and **14**, 1 µL for compounds **4** and **5**, 2 µL for compounds **8**, **12** and **13** and 3 µL for compounds **3**, **11**, **15** and **16**. The eluent was made from the following solvents: water (A) and methanol (B).

Wavelength = 239 nm (**4**, **12**, **14**), 253 nm (**5**, **8-10**), 328 nm (**13**), 338 nm (**11**), 341 nm (**3**, **15** and **16**).

Method D: Octadecylsilica was used as the stationary phase (Zorbax Eclipse Plus C18 4.6 x 150 mm, 1.8 µ, S.N. USWKY01594). Compounds were dissolved in methanol. The final concentrations were ~ 1 mg/mL, and the injection volume was 0.5 µL for compounds **4**, **5**, **9**, **10**, **13** and **14**, and 1 µL for compounds **3, 8, 11, 12, 15** and **16**. The eluent was made from the following solvents: water (A) and acetonitrile (B). Wavelength = 239 nm (**4, 5, 8-10** and **12-14**), 338 nm (**11**), 341 nm (**3**, **15** and **16**).

All compounds were > 95% pure.

Synthesis

Refer to Supporting Information for individual procedures, yields and characterization. Only General procedures follow:

General procedure for the preparation of 1,7-bis(alkylamino)-4,10-diazachrysenes

Compound **17**[31] and an excess of the appropriate amine were dissolved in NMP in a MW cuvette under argon. The reaction mixture was subjected to MW irradiation using *Biotage Initiator 2.5* apparatus for 6 h at 180 ºC. The cooled reaction mixture was poured onto ice-water. The obtained precipitate was filtered, washed with water, and dried under reduced pressure.

General procedure for the preparation of 1,7-bis(alkylamino)-4,10-diazachrysene hydrochlorides

The appropriate base was suspended in 40% HCl in dry MeOH, and the reaction mixture was vigorously stirred for 1 h at r.t. The solvent was then removed under reduced pressure, and the remaining solid was suspended in dry EtOH. The EtOH was removed under reduced pressure, and the same procedure with EtOH was repeated two more times. Upon drying at 40 ºC under reduced pressure, the desired product was obtained.

General procedure for the preparation of alkylaminonaphthyridines.

An appropriate chloronaphthyridine and the excess of appropriate amine were dissolved in NMP in a MW cuvette under argon. The reaction mixture was subjected to MW irradiation using *Biotage Initiator 2.5* apparatus for 2 hours at 180 ºC. The excess of amine and NMP were removed under reduced pressure using Kugelrohr device. The crude product was purified by column chromatography (dry flash, SiO_2, eluent DCM 100%, DCM/MeOH, gradient 9:1→1:9, MeOH 100%, MeOH/NH_4OH gradient 99:1 → 8:2), unless specified otherwise.

In Vitro Plasma Protein Binding.

Human serum albumin (HSA), alpha-1-acid glycoprotein (AGP), potassium dihydrogen phosphate, disodium hydrogen phosphate, sodium chloride, potassium chloride, and DMSO were purchased from Sigma-Aldrich. Fluorescence spectra were recorded on Horiba Jobin Yvon Fluoromax-4 spectrometer, equipped with Peltier element and magnetic stirrer for cuvette, using quartz cell with 1 cm path length and 4 mL volume. UV/vis spectra were recorded on a Thermo Scientific Evolution 60S spectrophotometer using quartz cell with 1 cm path length and 4 mL volume. All UV/vis spectra were recorded against the corresponding blank in the 200−500 nm wavelength range, with 500 nm/min scan speed. pH values were potentiometrically measured

using Crison pH-buret 24 2S equipped with a microcombined pH electrode (Crison pH electrode 50 29). The pH electrode was calibrated by standard Crisonbuffer solutions (pH 4.01, 7.00, and 9.21). Stock solutions of AGP ($c = 6.05\times10^{-5}$ M) and HSA ($c = 1.91\times10^{-4}$ M) were prepared in PBS (1×, pH 7.34) and kept in the refrigerator. Stock solutions of compounds were prepared in DMSO. For protein-compound interaction studies, protein solutions were freshly prepared from the stock by dilution with a buffer (AGP and HSA concentration was kept constant, $c=5\times10^{-7}$ M) and titrated with compound stock solution (from 1 to 20 compound/protein molar ratio). During the titration, the solutions were stirred and thermostated (t=25.0±0.1°C, regulated by Peltier element). The equilibration time between increment additions was 10 min. An excitation wavelength was 280 nm, with 5 nm slits; emission spectra were recorded in 300−450 nm wavelength range, with 5 nm slits and 0.1 s integration time. Background PBS signal was subtracted from each spectrum. Fluorescence intensities were corrected for inner filter effect by measuring absorbances at excitation and emission wavelength.

Cells and Cell culture

HeLa cells (ATCC) and Human Foreskin fibroblasts (HFF) cells (ATCC) were maintained at 37 ^{o}C in a 5% CO_2 in Minimum Essential Medium (MEM) (Corning Cellgro) supplemented with 10% fetal bovine serum (FBS, Hyclone).

Viruses

EBOV/ H. sapiens-wt/1995/Kikwit-9510621 (reference genome GenBank # KT582109; EBOV) from the stocks at United States Army Medical Research Institute of Infectious Diseases

(USAMRIID) were used for infection and were conducted under biosafety level 4 (BSL-4) conditions at USAMRIID.

High Content Image Based Quantification of EBOV infection and Other Phenotypes

Cells infected with EBOV were fixed in 10% formalin (Val Tech Diagnostics) for 24 h at room temperature. Cells were then immunofluorescently stained to visualize EBOV-GP expression using murine monoclonal antibody against EBOV (6D8), followed by Dylight488-conjugated goat anti-mouse IgG (ThermoFisher Scientific) in blocking buffer containing 3% bovine serum albumin (Sigma) in phosphate buffered salt solution (PBS). DRAQ5 (Biostatus) was used to stain nuclei (for dose response curve analysis [DRA]). In some cases, infected cells were also stained with Hoechst 33342 and HCS CellMask Red (ThermoFisher Scientific) for nuclei and cytoplasm detection, respectively. Images were acquired on the Opera imaging instrument (model 3842 and 5025; PerkinElmer) using ×10 air (for DRA), ×20 water, or ×40 water objective lenses as required. 4-20 images per well were acquired as described for each experiment. The total number of cells (based on nuclear staining) and the number of infected cells (based on GP positive cells) were determined using the Acapella (Perkin Elmer) image analysis software. In some cases, for higher resolution, images were acquired on Leica TCS-SP5 confocal/multiphoton microscope.

Dose response curve analysis (DRA)

The compound's activity against EBOV including EC_{50} or EC_{90}, which is the effective concentration to achieve 50% or 90% infection inhibition respectively, and CC_{50} (50% cytotoxicity) was accomplished by running the dose response curve analysis. Briefly, the compounds were tested in a 10-point dose-response curve assay at 2-fold serial dilution starting from 10 µM in 4 replicates (n-4) on the same plate. Table 1 represents data from one of the two experimental repeats performed on two consecutive days. Briefly, HeLa cells were seeded at 2000 cells per well in 35 µL of culture media into imaging 384-well assay plates (IQ-EB, Aurora) using the automated Multidrop^{TM} Combi dispenser (cat # 5840300, ThermoFisher Sceintific). After an overnight incubation at 37 °C, cells were pre-treated at 2 h with the compounds using automated HP-D300 with each dose dispensed directly from the concentrated stocks (10 mM). Cells were then infected with EBOV (MOI=0.5) for 48 h followed by IFA to detect EBOV-GP expressing cells. Images were acquired (4 images/well) and subjected to image analysis as described in the above sections to enumerate the number of cells and infected cells. Data was further evaluated by GeneData Explorer software as follows. The percentage (%) of virus positive cells associated with each well was converted into percentage inhibition using median data from control wells as follows.

NC = Neutral control (16 wells/ plate); Infection + DMSO (mock vehicle treatment)

BC = Blank control (16 wells/plate); No infection (false positives due to background noise from antibody staining)

$$\%\ \text{Inhibition} = \frac{\text{Median \% Virus Positive (NC)} - \text{\% Virus Positive (S)}}{\text{Median \% Virus Positive (NC)} - \text{\% Virus Positive (BC)}} * 100$$

Similarly, % Cell Viability was calculated using the following equation, that calculates the number of cells in a well relative to the number of cells in infected wells that were mock treated with DMSO (vehicle control)

$$\%\ \text{Cell Viability} = \frac{\text{Nuclei Number}}{\text{Median Nuclei Number (NC)}} * 100$$

The % Inhibition and the % Cell Viability was then used to determine the $EC_{50,}$ EC_{90} and CC_{50} values by applying the GeneData Condoseo software with LevenbergMarquardt algorithm (LMA) for curve fitting strategy. The Curve-fitting applied validity criteria, such aschi2, SE logEC_{50}, minimal number of valid data points, to indicate if curve fitting converging was successful as indicated in Table 1. R2 value quantifies goodness of fit. Fitting strategy was considered acceptable if R2 >0.8. The relative effectiveness of the compound is defined in terms of its selectivity index (SI), a value that indicates the relationship between the compound's effective and toxic concentrations, and is calculated as: $SI=CC_{50}/EC_{50}$. It is therefore desirable for a compound to have a high SI value, indicating maximum antiviral activity and minimal cell toxicity

In Vivo Efficacy Studies against EBOV Infection

To test the in vivo efficacy of the compounds against EBOV, mice (BALB/c; *n* =10/group) about 6-7 weeks old, were mock treated (vehicle control) or with the indicated concentrations of the compounds **2**, **4** or **13** via the intraperitoneal (IP) route and after 2 h were infected via the IP route with 1000 plaque forming units (PFU) of the mouse adapted strain of EBOV (Mayinga variant). The treatment was continued daily for 6 days. Mice survival was monitored for 14 days.

All the tested compounds have a solubility of ≥25 mg/mL in deionized water. The Kaplan–Meier survival curves are generated by GraphPad Prism software. P values were evaluated by comparing survival curves of individual doses with the control group using the log-rank test.

All mouse research were conducted under an IACUC-approved protocol in compliance with the Animal Welfare Act, PHS Policy, and other Federal statutes and regulations relating to animals and experiments involving animals. The facility where this research was conducted is accredited by the Association for Assessment and Accreditation of Laboratory Animal Care, International and adheres to principles stated in the Guide for the Care and Use of Laboratory Animals, National Research Council, 2011.

Time of Compound Addition Assay (TCA)

HeLa cells were seeded at 2×10^4 cells per well in a 96-well plate. Next day cells were either mock-infected or treated with compound 2 h prior to infection (pre), concurrent with virus infection (0 h), or at various time points post-infection as indicated in the experiment. Cells were infected with EBOV MOI=10. After 24 h, cells were subjected to IFA followed by HCA to determine the percentage of EBOV-GP expressing cells. Experiments were performed in triplicate and the average (± standard deviation) of two independent experiments is shown.

Viral Entry Assay with Pseudotyped Virus

Infectious recombinant vesicular stomatitis virus (rVSV) expressing the green fluorescent protein (GFP, [rVSV-GFP]) was a kind gift from Dr. John Connor [Boston University]) and rVSV-GFP in which the VSV GP was replaced with EBOV-GP (GP cDNA derived from

Mayinga isolate) was a kind gift from Dr. Kartik Chandran.[58] The virus was propagated in Vero E6 cells and the infections were performed under BSL-2 conditions. Briefly, cells were infected with viruses at MOI=0.1 and the supernatants were collected at day 3-4 when >50% of cells became cytopathic. The virus containing supernatants were clarified and stored at -80 ^{o}C. To titer the virus, different volumes of virus supernatants were used to infect HeLa cells in a 96 well plate, starting from 100 µL and serially diluted 20 times at 2/3-fold dilutions to determine the optimal volume of virus required to achieve 60-70% infection rates. We also determined the time take taken to observe the initial GFP expression even before the virus completes one life cycle using live cell imaging (images recorded every 15 minutes) on Opera. A time period of 8 h and 6 h with rVSV-EBOV-GP and rVSV-GFP respectively was determined to be optimal for capturing all cells expressing GFP within the first cycle of infection. The infections were scored by determining the percentage of GFP expressing cells using HCA. Cells and nuclei were stained with Cell MaskDeep Red. To determine the compounds effect on EBOV entry, HeLa cells in 96 well plates were pre-treated at 2 h with DMSO (vehicle control) or the indicated concentrations of various compounds prior to incubation with rVSV-GFP (10 µL) or rVSV-EBOV-GP-GFP (50 µl) viruses in triplicates and the infections were stopped by formalin treatment at 6 h and 8 h post infection respectively. This duration of infection was just enough to ensure early stages of viral infection including viral entry and replication (as indicated by GFP expression) but not virus egress.[80] Infections were scored by the enumeration of GFP expressing cells by HCA.

ACCEPTED MANUSCRIPT

Visualizing Acidic Compartments and Compounds

Acidic compartments were monitored by live cell imaging using LysoSensor DND 189 (ThermoFisher Scientific) or Acridine Orange ([AO], ImmunoChemistry). Cells were mock treated or pre-treated with the compounds at the times indicated in the experiment. Cells were then incubated with the LysoSensor probe or AO at 0.5 µM and incubated at 37 ^{o}C for 30 min. Cells were washed, replaced with fresh media and imaged by confocal microscopy. LysoSensor was detected at an excitation of (Ex.443 nm) and emission of (Em.505 nm). Monomeric AO (bound to nucleic acids) in green channels was visualized by Ex. 460-490 nm and Em. 520-560 nm while the dimerized and oligomerized AO in red channel (acidic compartments) were visualized with Ex. 520-560 nm and Em. 590-640 nm. The compounds **1** and **2** were florescent and after scanning for optimal absorbance and excitation, they were imaged at Ex/Em of 405/450 nm. At this emission, there was minimal or no bleed through by other reporters used in the study.

Cathepsin B Activity

Magic Red Cathepsin-B Assay (ImmunoChemistry) was used for detecting cathepsin activity by live cell imaging. The Magic Red substrate freely diffuses into cells and emits red fluorescence upon cleavage by active cathepsin B. The experiment was done as following the manufacturer's protocol. Briefly, cells were pre-treated with vehicle control (mock) or the compounds for a specific duration of time as indicated in the experiment. Cathepsin B substrate was then added to cells at a final dilution of 1:260 fold. Cells were incubated for 1 h at 37 ^{o}C followed by washes and imaging at Ex/Em of 590/620 nm.

Statistical Analysis

As indicated for each experiment, P values were evaluated by One Way Anova analysis, ir multiple t tests. ***, $P < 0.001$. **, $P < 0.01$.

Autophagy Detection

HeLa-GFP-LC3 stable cell line was generated by retroviral transduction using pBABE-GFP-LC3 (gift from Jayanta Debnath [Addgene plasmid # 22405]).[81] Cells were selected on Puromycin ([2 µg/mL], Sigma) for seven days. Cells were then sorted to select only medium to low LC3-GFP expressing cells and then analyzed for reporter activity. These cells were used for all experiments described. For imaging GFP-LC3 clusters, cells were seeded in 96 well plates, and the following day, cells were treated with compounds in 8 replicates at the concentrations described in the experiments for 6 h. Cells were then washed and imaged on Operetta at 20 X water objective at several Z planes to capture GFP clusters. Images from 20 fields per well and about 300 cells per well were acquired. The merged images were then analyzed for GFP clusters using Columbus software. Details of the script will be provided upon request and are similar to our previously described analysis.[82]

For western blot analysis, HeLa-GFP-LC3 cells were counted and seeded at same numbers in 12 well dishes. The following day, cells were treated with the indicated compounds for 6 h followed by cell lysis in 100 ml of 1.25X Laemmli sample loading buffer (ThermoScientific) and boiled for 5 min at 95 °C. Proteins were separated by SDS-PAGE, followed by transfer to a polyvinylidene (PVDF) membrane. The blots were incubated for 1h at RT or overnight at 4°C

with the indicated primary antibodies. After three washes, the blots were incubated with the appropriate alkaline phosphatase (AP)-conjugated secondary antibodies (GE Healthcare) according to the manufacturer's recommendations. The blots were washed and developed by a Western blotting detection system (GE Healthcare). The following antibodies were used for Western blot analysis: LC3 (Abcam), GFP (BD Transduction), GAPDH (Cell Signaling), and alkaline phosphatase (AP) conjugated secondary antibodies (ThermoScientific).

Electron Microscopy

HeLa cells grown on a 6 well dish were treated with the compounds for 2 h followed by infection with rVSV-EBOV-GP-GFP (MOI = 100) at the indicated duration of time. Cells were fixed for 1 h in primary fixative (2.5% formaldehyde, 2.5% glutaraldehyde, 0.1 M sodium cacodylate, pH 7.4) and scraped off the plates to collect cell pellets. Cells were then washed three times in ice-cold 0.1 M sodium cacodylate buffer, and incubated with 1% osmium tetroxide in 0.1 M of sodium cacodylate for 1 h, washed three times with distilled water, stained and stabilized on ice with 2% uranyl acetate for 1 h and successively dehydrated on ice through a series of 22%, 50%, 75%, and 95% ethanol. The cells were then dehydrated three times at room temperature in 100% ethanol and infiltrated in well-mixed 50% ethanol and 50% Durcupan ACM resin (Fluka, Sigma-Aldrich) for 1 h with agitation. Cells were infiltrated twice by 100% Durcupan ACM for 3 h with agitation, after which the samples were placed in an oven and polymerized at 60 °C for at least 48 h. Thin sections (approximately 80 nm) were collected and pre-stained with 1% uranyl acetate and Sato lead before examination on a JEOL 1011

transmission electron microscope at 80 kV. Digital images were acquired using an AMT camera system.

AUTHOR INFORMATION

Corresponding Author

*For B.Š.: phone, +381-11-263-86-06; fax, +381-11-263-60-61;

E-mail: bsolaja@chem.bg.ac.rs; bogdan.solaja@sanu.ac.rs.

*For R.M.: phone, +1-301 619-8016; Fax: +1-301 619-0350;

E-mail: rajini.r.mudhasani.ctr@mail.mil.

ORCID

Bogdan A. Šolaja: https://orcid.org/0000-0002-9975-2725

Author Contributions

B.Š. and R.M. designed the research. The results are part of the projected dissertation of Ž.S., University of Belgrade. The manuscript was written by Ž.S., R.M. and B.Š. All authors have given approval to the final version of the manuscript.

ACCEPTED MANUSCRIPT

Notes

Opinions, interpretations, conclusions, and recommendations stated within the article are those of the authors and are not necessarily endorsed by the U.S. Army nor does mention of trade names, commercial products, or organizations imply endorsement by the U.S. Government. The authors declare no competing financial interest.

ACKNOWLEDGMENT

This research was supported by the National Institute of Allergy and Infectious Diseases (U.S.) Grant 5-U01AI082051-02 (SB, BŠ) and in part by the Department of Defense Chemical Biological Defense Program through the Defense Threat Reduction Agency (DTRA) under United States Army Medical Research Institute of Infectious Diseases (USAMRIID) (project number 13255634), and by the Ministry of Science and Technological Development of Serbia Grant 172008 (ŽS, TV, BŠ), Serbian Academy of Sciences and Arts (BŠ). We thank Dr. Olgica Đurković-Đaković and MSc Jelena Srbljanović (Institute for Medical Research, University of Belgrade) for help with collecting mice blood samples for pharmacokinetics and performing in vivo toxicity studies. We thank Dr. Jelena Konstantinović (Faculty of Chemistry, University of Belgrade) for help with the setup of pharmacokinetics experiments and data interpretation. We thank Dr. Benedict Capacio and colleagues at the ADME Center at the US Army Medical Institute for Chemical Defense for evaluating the ADME properties of our compounds. We thank Tara Kenny for providing HFF cells.

ACCEPTED MANUSCRIPT

ABBREVIATIONS

AO – acridine orange; AQ – amodiaquine; CAD – cationic amphiphilic drug; CQ – chloroquine; CYP – Cytochrome P450; EBOV – Ebola virus; EM – electron microscopy; Em – emission; EVD – Ebola virus disease; Ex – excitation; GFP – green fluorescent protein; GP – glycoprotein; HCS – high-content screening; HeLa – cervical cancer immortal cell line from a 30-year-old female patient named Henrietta Lacks; HFF – human foreskin fibroblasts; HOPS – homotypic fusion and protein sorting; hpf – hours post fertilization; LC3 – Microtubule-associated proteins 1A/1B light chain 3B; LE – late endosome; MDCK – Madin-Darby Canine Kidney cells, a kidney tubule cell line from a Cocker Spaniel dog; MOA – mechanism of action; MOI – multiplicity of infection; HNP – non-human primates; NPC1 – Niemann-Pick disease type C1 (protein); PFU – plaque forming units; Pgp – P-glycoprotein; RNP – ribonucleoprotein complex; (r)VSV – (recombinant) vesicular stomatitis virus; SNARE – soluble NSF (*N*-ethylmaleimide-sensitive factor) attachment protein receptor; TCA – time of compound addition

ASSOCIATED CONTENT

Supporting Information.

The following files are available free of charge.

Supporting information – I, PDF

Spectral and analytical data for all synthesized compounds; detailed procedures for the determination of the HPLC purity. Brief descriptions of cell based assays. ADME data.

Fluorescence and UV-Vis spectra for determination of binding to HSA and AGP. In vivo mouse pharmacokinetics. pKa value determination; Zebrafish model toxicity; mouse model toxicity.

Supporting information – II, PDF

NMR spectra and HPLC purity spectra of all tested compounds.

References

[1] WHO Situation report, June 10th, 2016: http://apps.who.int/iris/bitstream/10665/208883/1/ebolasitrep_10Jun2016_eng.pdf?ua=1 (accessed 24 August 2018)

[2] WHO Factsheet: Chronology of previous Ebola virus disease outbreaks:

http://www.who.int/mediacentre/factsheets/fs103/en/ (accessed 24 August 2018)

[3] Ebola virus disease – Democratic Republic of the Congo. WHO: http://www.who.int/csr/don/17-august-2018-ebola-drc/en/. (accessed 24 August 2018)

[4] K. Brauburger, A.J. Hume, E. Muhlberger, J. Olejnik, Forty-five years of Marburg virus research, Viruses 4 (2012) 1878−1927.

[5] K.J. Olival, D.T.S. Hayman, Filoviruses in bats: current knowledge and future directions, Viruses 6 (2014) 1759-1788.

[6] L. Baseler, D.S. Chertow, K.M. Johnson, H. Feldmann, D.M. Morens, The pathogenesis of Ebola virus disease, Annu. Rev. Pathol. Mech. Dis. 12 (2017) 15.1–15.32.

[7] J.E. Ledgerwood, et al. Chimpanzee Adenovirus vector Ebola vaccine, N. Engl. J. Med. 376 (2017) 928-938.

[8] A.M. Henao-Restrepo, et al. Efficacy and effectiveness of an rVSV-vectored vaccine in preventing Ebola virus disease: final results from the Guinea ring vaccination, open-label, cluster-randomised trial (Ebola Ça Suffit!), The Lancet 389 (2017) 505-518.

[9] R.L. Winslow, I.D. Milligan, M. Voysey, K. Luhn, G. Shukarev, M. Douoguih, M.D. Snape, Immune responses to novel Adenovirus type 26 and modified vaccinia virus Ankara-vectored Ebola vaccines at 1 Year, JAMA 317 (2017) 1075-1077.

[10] J. Cohen, Research during Ebola vaccine trial: It's complicated, Science, 2018, doi:10.1126/science.aau2942.

[11] L. Oestereich, A. Lüdtke, S. Wurr, T. Rieger, C. Muñoz-Fontela, S. Günther, Successful treatment of advanced Ebola virus infection with T-705 (favipiravir) in a small animal model, Antiviral Research 105 (2014) 17-21.

[12] Sissoko, D., Laouenan, C., Folkesson, E., M'Lebing, A.-B., Beavogui, A.-H., Baize, S., et al., 2016. Experimental treatment with favipiravir for Ebola virus disease (the JIKI Trial): A historically controlled, single-arm proof-of-concept trial in Guinea. PLoS Med. 13, e1001967.

[13] Johansen, L.M., Brannan, J.M., Delos, S.E., Shoemaker, C.J., Stossel, A., Lear, C., Hoffstrom, B.G., Evans DeWald, L., Schornberg, K.L., Scully, C., Lehár, J., Hensley, L.E., White, J.M., Olinger, G.G., 2013. FDA-approved selective estrogen receptor modulators inhibit Ebola virus infection. Sci Transl Med. 5, 190ra79.

[14] Y. Zhao, J. Ren, K. Harlos, D.M. Jones, A. Zeltina, T.A. Bowden, S. Padilla-Parra, E.E. Fry, D.I. Stuart, Toremifene interacts with and destabilizes the Ebola virus glycoprotein, Nature 535 (2016) 169–172.

[15] T.K. Warren, J. Wells, R.G. Panchal, K.S. Stuthman, N.L. Garza, S.A. Van Tongeren, L/ Dong, C.J. Retterer, B.E. Eaton, G. Pegoraro, S. Honnold, S. Bantia, P. Kotian, X. Chen, B.R. Taubenheim, L.W. Welch, D.M. Minning, Y.S. Babu, W.P. Sheridan, S. Bavari, Protection against filovirus diseases by a novel broad-spectrum nucleoside analogue BCX4430, Nature 508 (2014) 402−405.

[16] T.K. Warren, R. Jordan, M.K. Lo, A.S. Ray, R.L. Mackman, V. Soloveva, D. Siegel, M. Perron, R. Bannister, H.C. Hui, N. Larson, R. Strickley, J. Wells, K.S. Stuthman, S.A. Van Tongeren, N.L. Garza, G. Donnelly, A.C. Shurtleff, C.J. Retterer, D. Gharaibeh, R. Zamani, T. Kenny, B.P. Eaton, E. Grimes, L.S. Welch, L. Gomba, C.L. Wilhelmsen, D.K. Nichols, J.E. Nuss, E.R. Nagle, J.R. Kugelman, G. Palacios, E. Doerffler, S. Neville, E. Carra, M.O. Clarke, L. Zhang, W. Lew, B. Ross, Q. Wang, K. Chun, L. Wolfe, D. Babusis, Y. Park, K.M. Stray, I. Trancheva, J.Y. Feng, O. Barauskas, Y. Xu, P. Wong, M.R. Braun, M. Flint, L.K. McMullan, S.-S. Chen, R. Fearns, S. Swaminathan, D.L. Mayers, C.F. Spiropoulou, W.A. Lee, S.T. Nichol, T. Cihlar, S. Bavari, Therapeutic efficacy of the small molecule GS-5734 against Ebola virus in rhesus monkeys, Nature 531 (2016) 381-385.

[17] Ž. Selaković, D. Opsenica, B. Eaton, C. Retterer, S. Bavari, J.C. Burnett, B.A. Šolaja, R.G. Panchal, A limited structural modification results in a significantly more efficacious diazachrysene-based filovirus inhibitor, Viruses 4 (2012) 1279-1288.

[18] Madrid, P.B., Chopra, S., Manger, I.D., Gilfillan, L., Keepers, T.R., Shurtleff, A.C., Green, C.E., Iyer, L.V., Dilks, H.H., Davey, R.A., Kolokoltsov, A.A., Carrion, R., Patterson, J.L., Bavari, S., Panchal, R.G., Warren, T.K., Wells, J.B., Moos, W.H., Burke, R.L., Tanga, M.J., 2013. A systematic screen of FDA-approved drugs for inhibitors of biological threat agents. PLoS ONE. 8, e60579.

[19] Shoemaker, C.J., Schornberg, K.L., Delos, S.E., Scully, C., Pajouhesh, H., Olinger, G.G., Johansen, L.M., White, J.M., 2013. Multiple cationic amphiphiles induce a Niemann-Pick C phenotype and inhibit Ebola virus entry and infection. PLoS ONE. 8, e56265.

[20] Johansen, L.M., DeWald, L.E., Shoemaker, C.J., Hoffstrom, B.G., Lear-Rooney, C.M., Stossel, A., Nelson, E., Delos, S.E., Simmons, J.A., Grenier, J.M., Pierce, L.T., Pajouhesh, H., Lehár, J., Hensley, L.E., Glass, P.J., White, J.M., Olinger, G.G., 2015. A screen of approved drugs and molecular probes identifies therapeutics with anti-Ebola virus activity. Sci Transl Med. 7, 290ra89.

[21] W.H. Halliwell, Cationic amphiphilic drug-induced phospholipidosis, Toxicol. Pathol. 25 (1997) 53-60.

[22] K. Chandran, N.J. Sullivan, U. Felbor, S.P. Whelan, J.M. Cunningham, Endosomal proteolysis of the Ebola virus glycoprotein is necessary for infection, Science 308 (2005) 1643-1645.

[23] K. Schornberg, S. Matsuyama, K. Kabsch, S. Delos, A. Bouton, J. White, Role of endosomal cathepsins in entry mediated by the Ebola virus glycoprotein, J. Virol. 80 (2006) 4174-4178.

[24] M. Brecher, K.L. Schornberg, S.E. Delos, M.L. Fusco, E.O. Saphire, J.M. White, Cathepsin cleavage potentiates the Ebola virus glycoprotein to undergo a subsequent fusion-relevant conformational change, J Virol. 86 (2012) 364-372.

[25] J.E. Carette, M. Raaben, A.C. Wong, A.S. Herbert, G. Obernosterer, N. Mulherkar, A.I. Kuehne, P.J. Kranzusch, A.M. Griffin, G. Ruthel, P. Dal Cin, J.M. Dye, S.P. Whelan, K. Chandran, T.R. Brummelkamp, Ebola virus entry requires the cholesterol transporter Niemann-Pick C1, Nature 477 (2011) 340-343.

[26] M. Côté, J. Misasi, T. Ren, A. Bruchez, K. Lee, C.M. Filone, L. Hensley, Q. Li, D. Ory, K. Chandran, J. Cunningham, Small molecule inhibitors reveal Niemann-Pick C1 is essential for Ebola virus infection, Nature 477 (2011) 344-348.

[27] P.B. Madrid, R.G. Panchal, T.K. Warren, A.C. Shurtleff, A.N. Endsley, C.E. Green, A. Kolokoltsov, R. Davey, I.D. Manger, L. Gilfillan, S. Bavari, M.J. Tanga, Evaluation of Ebola virus inhibitors for drug repurposing, ACS Inf. Dis. 1 (2015) 317-326.

[28] S.D. Dowall, A. Bosworth, R. Watson, K. Bewley, I. Taylor, E. Rayner, L. Hunter, G. Pearson, L. Easterbrook, J. Pitman, R. Hewson, M.W. Carroll, Chloroquine inhibited Ebola virus replication in vitro but failed to protect against infection and disease in the in vivo guinea pig model, J Gen Virol. 96 (2015) 3484-3492.

[29] D. Falzarano, D. Safronetz, J. Prescott, A. Marzi, F. Feldmann, H. Feldmann, Lack of protection against Ebola virus from chloroquine in mice and hamsters, Emerg. Infect. Dis. 21 (2015) 1065-1067.

[30] E. Gignoux, A.S. Azman, M. de Smet, P. Azuma, M. Massaquoi, D. Job, A. Tiffany, R. Petrucci, E. Sterk, J. Potet, M. Suzuki, A. Kurth, A. Cannas, A. Bocquin, T. Strecker, C. Logue, T. Pottage, C. Yue, J.C. Cabrol, M. Serafini, I. Ciglenecki, Effect of Artesunate-Amodiaquine on mortality related to Ebola virus disease, N Engl J Med. 374 (2016) 23-32.

[31] Ž. Selaković, V. Soloveva, D. Gharaibeh, J. Wells, S. Šegan, R.G. Panchal, B.A. Šolaja, Anti-Ebola activity of diazachrysene small molecules, ACS Inf. Dis. 1 (2015) 264-271.

[32] T.J. Ritchie, S.J.F. Macdonald, The impact of aromatic ring count on compound developability - are too many aromatic rings a liability in drug design? Drug Discovery Today 14 (2009) 1011-1020.

[33] K. Yamada, A. Hakura, T.A. Kato, T. Mizutani, K. Saeki, Nitrogen-substitution effects on the mutagenicity and cytochrome P450 isoform-selectivity of chrysene analogs, Mutat. Res. 586 (2005) 87–95.

[34] A. Johns, R. Alan Porter, Cinnamide derivatives as orexin-1 receptors antagonists, Int. Patent 2000047576, August 17, 2000.

[35] A.C. Castro, C.A. Evans, S. Janardanannair, A. Lescarbeau, T. Liu, D.A. Snyder, M.R. Tremblay, P. Ren, Y. Liu, L. Li, K. Chan, Heterocyclic compounds and uses thereof, Int. Patent 2013012915, January 24, 2013.

[36] S.B. Brown, M.J.S. Dewar, Centrosymmetric 1,5-naphthyridine derivatives: synthesis, tautomerism, and thermal rearrangements, J. Org. Chem. 43 (1978) 1331-1337.

[37] D.P. Provencal, K.D. Gesenberg, H. Wang, C. Escobar, H. Wong, M.A. Brown, A.J. Staab, Y.R. Pendri, Development of an efficient and scalable process of a respiratory syncytial virus inhibitor, Org. Proc. Res. Dev. 8 (2004) 903–908.

[38] Y. Noritake, N. Umezawa, N. Kato, T. Higuchi, Manganese salen complexes with acid−base catalytic auxiliary: functional mimetics of catalase, Inorg. Chem. 52 (2013) 3653–3662

[39] R.G. Panchal, K.P. Kota, K.B. Spurgers, G. Ruthel, J.P. Tran, R.C. Boltz, S. Bavari, Development of high-content imaging assays for lethal viral pathogens, J. Biomol. Screening 15 (2010) 755−765.

[40] R. Mudhasani, K.P. Kota, C. Retterer, J.P. Tran, S.R. Tritsch, R. Zamani, C.A. Whitehouse, S. Bavari, High-content image-based screening of a signal transduction pathway inhibitor small-molecule library against highly pathogenic RNA viruses, J Biomol Screen. 20 (2015) 141-152.

[41] M.J. Aman, M.S. Kinch, K. Warfield, T. Warren, A. Yunus, S. Enterlein, E. Stavale, P. Wang, S. Chang, Q. Tang, K. Porter, M. Goldblatt, S. Bavari, Development of a broad-spectrum antiviral with activity against Ebola virus, Antiviral Research 83 (2009) 245-251.

[42] K. Lee, T. Ren, M. Côté, B. Gholamreza, J. Misasi, A. Bruchez, J. Cunningham, Inhibition of Ebola virus infection: identification of Niemann-Pick C1 as the target by optimization of a chemical probe, ACS Medicinal Chemistry Letters 4 (2013) 239-243.

[43] Department of Defense, ADMET Center at USAMRICD, Gunpowder, Maryland, USA.

[44] R. Punith, A.H. Hegde, S. Jaldappagari, Binding of an anti-inflammatory drug lornoxicam with blood proteins: insights from spectroscopic investigations, J. Fluoresc. 21 (2011) 487–495.

[45] F. Zsila, J. Visy, G. Mády, I. Fitos, Selective plasma protein binding of antimalarial drugs to α1-acid glycoprotein, Bioorg. Med. Chem. 16 (2008) 3759–3772.

[46] G. Schwertz, M.C. Witschel, M. Rottmann, R. Bonnert, U. Leartsakulpanich, P. Chitnumsub, A. Jaruwat, W. Ittarat, A. Schäfer, R.A. Aponte, S.A. Charman, K.L. White, A. Kundu, S. Sadhukhan, M. Lloyd, G.M. Freiberg, M. Srikumaran, M. Siggel, A. Zwyssig, P. Chaiyen, F. Diederich, Antimalarial inhibitors targeting serine hydroxymethyltransferase (SHMT) with in vivo efficacy and analysis of their binding mode based on X-ray cocrystal structures, Journal of Medicinal Chemistry 60 (2017) 4840-4860.

[47] ACD/Labs Release 12.0, ACD/PhysChem build 39480 - Advanced Chemistry Development, Inc. 8 King Street East, Suite 107, Toronto, Ontario, Canada M5C 1B5

[48] ADMET Predictor, Simulations Plus, Inc., Lancaster, CA, USA, ver. 8.5, 2017.

[49] R. Fraczkiewicz, M. Lobell, A.H. Göller, U. Krenz, R. Schoenneis, R.D. Clark, A. Hillisch, Best of both worlds: Combining pharma data and state of the art modeling technology to improve in silico pKa prediction, Journal of Chemical Information and Modeling 55 (2014) 389-397.

[50] J.M. Schulman, G.R. Strichartz, Local anesthetic pharmacology, in: D.E. Golan, A.H. Tashjian, E.J. Armstrong A.W. Armstrong (Eds.) Principles of Pharmacology: The

Pathophysiologic Basis of Drug Therapy, 3rd edition, LIPPINCOTT WILLIAMS & WILKINS, Philadelphia, 2012, pp. 147-163.

[51] Y. Zhang, L. Han, Q. He, W. Chen, C. Sun, X. Wang, X. Chen, R. Wang, C.-D. Hsiao, K. Liu, A rapid assessment for predicting drug-induced hepatotoxicity using zebrafish, Journal of Pharmacological and Toxicological Methods 84 (2017) 102-110.

[52] M. Bray, K. Davis, T. Geisbert, C. Schmaljohn, J. Huggins, A mouse model for evaluation of prophylaxis and therapy of Ebola hemorrhagic fever, J Infect Dis. 178 (1998) 651-661.

[53] T.K. Warren, K.L. Warfield, J. Wells, S. Enterlein, M. Smith, G. Ruthel, A.S. Yunus, M.S. Kinch, M. Goldblatt, M.J. Aman, S. Bavari, Antiviral activity of a small-molecule inhibitor of filovirus infection, Antimicrob Agents Chemother. 54 (2010) 2152-2159.

[54] P.L. Iversen, T.K. Warren, J.B. Wells, N.L. Garza, D.V. Mourich, L.S. Welch, R.G. Panchal, S. Bavari, Discovery and early development of AVI-7537 and AVI-7288 for the treatment of Ebola virus and Marburg virus infections, Viruses 4 (2012) 2806-2830.

[55] J. Chang, T.K. Warren, X. Zhao, T. Gill, F. Guo, L. Wang, M.A. Comunale, Y. Du, D.S. Alonzi, W. Yu, H. Ye, F. Liu, J.T. Guo, A. Mehta, A. Cuconati, T.D. Butters, S. Bavari, X. Xu, T.M. Block, Small molecule inhibitors of ER alpha-glucosidases are active against multiple hemorrhagic fever viruses, Antiviral Res. 98 (2013) 432-440.

[56] R.S. Funk, J.P. Krise, Cationic amphiphilic drugs cause a marked expansion of apparent lysosomal volume: implications for an intracellular distribution-based drug interaction, Mol Pharm. 9 (2012) 1384-1395.

[57] R.M. Mingo, J.A. Simmons, C.J. Shoemaker, E.A. Nelson, K.L. Schornberg, R.S. D'Souza, J.E. Casanova, J.M. White, Ebola virus and severe acute respiratory syndrome coronavirus display late cell entry kinetics: evidence that transport to NPC1+ endolysosomes is a rate-defining step, J Virol 89 (2015) 2931-2943.

[58] A.C. Wong, R.G. Sandesara, N. Mulherkar, S.P. Whelan, K. Chandran, A forward genetic strategy reveals destabilizing mutations in the Ebolavirus glycoprotein that alter its protease dependence during cell entry, J Virol. 84 (2010) 163-175.

[59] S.B. Sieczkarski, G.R. Whittaker, Differential requirements of Rab5 and Rab7 for endocytosis of influenza and other enveloped viruses, Traffic 4 (2003) 333-343.

[60] I. Opsenica, J.C. Burnett, R. Gussio, D. Opsenica, N. Todorović, C.A. Lanteri, R.J. Sciotti, M. Gettayacamin, N. Basilico, D. Taramelli, J.E. Nuss, L. Wanner, R.G. Panchal, B.A. Šolaja, S. Bavari, A chemotype that inhibits three unrelated pathogenic targets: the botulinum neurotoxin serotype A light chain, P. falciparum malaria, and the Ebola filovirus, J Med Chem. 54 (2011) 1157-1169.

[61] R.J. Wool-Lewis, P. Bates, Characterization of Ebola virus entry by using pseudotyped viruses: identification of receptor-deficient cell lines, J Virol. 72 (1998) 3155-3160.

[62] F.R. Maxfield, D.J. Yamashiro, Endosome acidification and the pathways of receptor-mediated endocytosis, Adv Exp Med Biol. 225 (1987) 189-198.

ACCEPTED MANUSCRIPT

[63] H. Tapper, R. Sundler, Bafilomycin A1 inhibits lysosomal, phagosomal, and plasma membrane H(+)-ATPase and induces lysosomal enzyme secretion in macrophages, J Cell Physiol. 163 (1995) 137-144.

[64] M.P. Thome, E.C. Filippi-Chiela, E.S. Villodre, C.B. Migliavaca, G.R. Onzi, K.B. Felipe, G. Lenz, Ratiometric analysis of Acridine Orange staining in the study of acidic organelles and autophagy, J Cell Sci. 129 (2016) 4622-4632.

[65] L. Zilbermintz, W. Leonardi, S.Y. Jeong, M. Sjodt, R. McComb, C.L. Ho, C. Retterer, D. Gharaibeh, R. Zamani, V. Soloveva, S. Bavari, A. Levitin, J. West, K.A. Bradley, R.T. Clubb, S.N. Cohen, V. Gupta, M. Martchenko, Identification of agents effective against multiple toxins and viruses by host-oriented cell targeting, Sci Rep. 5 (2015) 13476.

[66] J.J. Lum, D.E. Bauer, M. Kong, M.H. Harris, C. Li, T. Lindsten, C.B. Thompson, Growth factor regulation of autophagy and cell survival in the absence of apoptosis, Cell 120 (2005) 237-248.

[67] M.L. Goodall, T. Wang, K.R. Martin, M.G. Kortus, A.L. Kauffman, J.M. Trent, S. Gately, J.P. MacKeigan, Development of potent autophagy inhibitors that sensitize oncogenic BRAF V600E mutant melanoma tumor cells to vemurafenib, Autophagy 10 (2014) 1120-1136.

[68] K. Yamasaki, V.T.G. Chuang, T. Maruyama, M. Otagiri, Albumin-drug interaction and its clinical implication, Biochim. Biophys. Acta, Gen. Subj. 1830 (2013) 5435−5443.

[69] Z.H. Israili, P.G. Dayton, Human alpha-1-glycoprotein and its interactions with drugs, Drug Metab. Rev. 33 (2001) 161−235.

[70] D.A. Smith, L. Di, E.H. Kerns, The effect of plasma protein binding on in vivo efficacy: misconceptions in drug discovery, Nat. Rev. Drug Discovery 9 (2010) 929−939.

[71] Kouznetsova, J., Sun, W., Martínez-Romero, C., Tawa, G., Shinn, P., Chen, C.Z., Schimmer, A., Sanderson, P., McKew, J.C., Zheng, W., García-Sastre, A., 2014. Identification of 53 compounds that block Ebola virus-like particle entry via a repurposing screen of approved drugs. Emerg Microbes Infect. 3, e84.

[72] E.A. Nelson, A.B. Barnes, R.D. Wiehle, G.K. Fontenot, T. Hoenen, J.M. White, Clomiphene and its isomers block Ebola virus particle entry and infection with similar potency: potential therapeutic implications, Viruses 8 (2016) 206.

[73] C. Salata, A. Calistri, C. Parolin, A. Baritussio, G. Palù, Antiviral activity of cationic amphiphilic drugs, Expert Rev Anti Infect Ther. 15 (2017) 483-492.

[74] S. Nadanaciva, S. Lu, D.F. Gebhard, B.A. Jessen, W.D. Pennie, Y. Will, A high content screening assay for identifying lysosomotropic compounds, Toxicol. In Vitro 25 (2011) 715-723.

[75] Lu, S., Sung, T., Lin, N., Abraham, R.T., Jessen, B.A., 2017. Lysosomal adaptation: How cells respond to lysosomotropic compounds. PLoS One. 12, e0173771.

[76] R. Logan, A.C. Kong, E. Axcell, J.P. Krise, Amine-containing molecules and the induction of an expanded lysosomal volume phenotype: a structure-activity relationship study, J Pharm Sci, 103 (2014) 1572-1580.

[77] Y. Sakurai, A.A. Kolokoltsov, C.C. Chen, M.W. Tidwell, W.E. Bauta, N. Klugbauer, C. Grimm, C. Wahl-Schott, M. Biel, R.A. Davey, Ebola virus. Two-pore channels control Ebola virus host cell entry and are drug targets for disease treatment, Science 347 (2015) 995-998.

[78] P. Jiang, T. Nishimura, Y. Sakamaki, E. Itakura, T. Hatta, T. Natsume, N. Mizushima, The HOPS complex mediates autophagosome-lysosome fusion through interaction with syntaxin 17, Mol. Biol. Cell. 25 (2014) 1327-1337.

[79] J.A. Shayman, A. Abe, Drug induced phospholipidosis: an acquired lysosomalstorage disorder, Biochim Biophys Acta. 1831 (2013) 602-611.

[80] M. Garbutt, R. Liebscher, V. Wahl-Jensen, S. Jones, P. Möller, R. Wagner, V. Volchkov, H.D. Klenk, H. Feldmann, U. Ströher, Properties of replication-competent vesicular stomatitis virus vectors expressing glycoproteins of filoviruses and arenaviruses, J Virol. 78 (2004) 5458-5465.

[81] C. Fung, R. Lock, S. Gao, E. Salas, J. Debnath, Induction of autophagy during extracellular matrix detachment promotes cell survival, Mol Biol Cell 19 (2008) 797-806.

[82] Mudhasani, R., Kota, K.P., Retterer, C., Tran, J.P., Whitehouse, C.A., Bavari, S., 2014. Highcontent image-based screening of a protease inhibitor library reveals compounds broadly active against Rift Valley fever virus and other highly pathogenic RNA viruses. PLoS Negl Trop Dis. 8, e3095.

ACCEPTED MANUSCRIPT

1. Second generation diazachrysene protects mice from Ebola virus
2. Naphthyridines are a new class of compounds active against Ebola virus
3. Favorable pharmacokinetics, tolerability and efficacy in *in vivo* mouse models
4. Mechanism of action tied to acidic compartment; host based; shows unique features
5. Diazachrysene enhances vesicle expansion and enables virus internalization

ACCEPTED MANUSCRIPT